Title
A New Synthetic Approach for Construction Acid-Base Heterogeneous Tandem Catalysts

Author
Yu, Tianyi

Publication Date
2020

Peer reviewed|Thesis/dissertation

UNIVERSITY OF CALIFORNIA
RIVERSIDE

A New Synthetic Approach for Construction Acid-Base Heterogeneous Tandem Catalysts

A Dissertation submitted in partial satisfaction
of the requirements for the degree of

Doctor of Philosophy

in

Chemistry

by

Tianyi Yu

December 2020

Dissertation Committee:
Dr. Francisco Zaera, Chairperson
Dr. Ludwig Bartels
Dr. Matthew Conley

The Dissertation of Tianyi Yu is approved:

Committee Chairperson

University of California, Riverside

ACKNOWLEDGEMENTS

First, the text in Chapter 2 of this dissertation, in part, is a reprint of the material as it appears in ACS Catal. 2018, 8, 2870−2879. The co-author, Zhihuan Weng, listed in that publication directed and supervised the research which forms the basis for this dissertation.

Foremost, I would like to thank my supervisor, Dr. Francisco Zaera, for giving me a chance to be one part of his research group, as well as guiding me onto the path towards a chemist. Frankly, I had to concede that I am not a genius student and will sometimes make mistakes, but you still showed me great patience and guidance without reservation. It's kind of hard to express my thank with my non-native language, but what I've gained from our lab and from you are invaluable in my career life and will inspire me forever. I would also like to thank my committee members, Dr.Ludwig Bartels and Dr. Matthew Conley, for their kindly support and guidance throughout this research.

Special thanks to my girlfriend, Scarlet, and my family in China. They supported my five years Ph.d life with their best and sometimes had to face my bad temper. I feel really blessed to have you in my life.

Although people always say no need to say thank you to your friends, I still want to thank my friends: Claire, Eva, Fan, Hana, Dr. Geson, Leo…, especially for Hana, who granted my great patience. Graduate life is tough. I won't get it over without all of you.

It's my great honor to work with Dr.Ilkeun, Tongxin and all the other researchers in our lab. We share creative idea together and help each other with both lab issue and daily life.

ABSTRACT OF THE DISSERTATION

A New Synthetic Approach for Construction Acid-Base Heterogeneous Tandem Catalysts

by

Tianyi Yu

Doctor of Philosophy, Graduate Program in Chemistry
University of California, Riverside, December 2020
Dr. Francisco Zaera, Chairperson

The aim of this thesis proposed here is to design a novel, universal route of constructing a solid-phase catalytic system, which presents an acid-base multifunctional property. Such a catalytic system is capable of selectively promoting multiple one-pot tandem reactions(e.g. Deacetalization-Henry reaction, Cyano-Ethoxycarbonylation reaction……). The heterogeneous systems we utilized to perform tandem reactions would be chemically incompatible if carried out in solution or in multiple separate stages. A commercially available mesoporous silica, SBA-15, was used as support in this thesis and the spatial separation of two functional groups was achieved using known grafting chemistry followed by Ultra-violet/Ozonolysis treatment (Uv/O_3).

In the second chapter, a combination of simplest base, amino group (NH_2-), and sulfonic acid (HSO_3-) group was grafted onto commercial mesoporous SBA-15. The resulting catalyst was investigated by multiple characterization methods such as solid-state ^{13}C, ^{29}Si

cross-polarization magic-angle spinning (CP/MAS) NMR, Fourier-transform infrared spectrometer, and N_2 adsorption−desorption isotherms. Those data indicated both functional groups were successfully tethered onto SBA15 and original mesoporous structure was maintained well.

Monitored by Gas-Chromatograph, the catalytic performance for a series of NH_2-HSO_3-SBA15 catalyst was examined in the second Chapter via Deacetalization-Henry reaction. Physical mixture and mono-functionalized catalysts (NH_2 grafted SBA-15 and HSO_3 grafted SBA-15) were tested as comparison groups as well. The result further confirmed the successfully grafting work of combining and separating both acid and base onto one support.

The third chapter deals with a new acid-base system, a phosphonic acid-cinchonidine bifunctional catalyst. Besides all techniques previously applied, solid state ^{31}P cross-polarization magic-angle spinning (CP/MAS) NMR and CNS Flash elemental analysis were further introduced to characterize those more complicated parts. A bimodal-shaped pore size also revealed that Uv/ozonolysis process was slow but tunable by controlling the treatment length.

Due to new functionalities introduced by grafting cinchonidine group, the new system was further capable of a couple of new reactions. Three reactions were then successfully tested: Deacetalization-Henry cascade reaction, Cyano-Ethoxycarbonylation reaction, and 1,4-addition of thiols to cylic enones. The result confirmed the successful construction work of grafting new acid and base groups. However, a loss in enantioselectivity has been observed here. It may cause by the non-chirality of tethered acid sites.

Table of Contents

Chapter 1: Introduction: Hybrid Organic-Inorganic Materials and Multifunctional Heterogeneous catalysts

The increasing of energy demands nowadays lead scientist to the area of "Green Chemistry". As the report from the International Energy Agency in 2013 shown, in the chemicals sector energy consumption would increase from 42 exajoules (EJ) in 2010 to 85 EJ in 2050.[1] Anyway, improvements in catalysis and related field could significantly reduce energy intensity for these products by 20% to 40% as a whole by 2050, as much as 13 EJ. Besides, the reduction of the environmentally deleterious effects in such processes accomplished by multistep, single-vessel catalysis cannot be discounted which is mostly caused by excess use of solvents during purification steps. Ideally, even if such processes require multiply steps, those syntheses should also be done with one catalytic system and in one-pot. By introducing such a combined system, people will reduce the isolation and purification step required which leads to not only less waste produced and less use of solvent, but also a significant amount of energy saving because of the elimination of heat-based process(i.e., evaporation, recrystallization….).[2]

How to design such a multifunctional system, especially when the concepts of green chemistry are involved, becomes a critical problem to scientists. Unfortunately, combining catalytic functional groups in solution is often limited by chemical incompatibilities between different components, such as one of the most common pairs, acid and base. Besides, other problems like separation and recycle of catalyst are also inevitable for homogenous bifunctional catalysts. In this project, we will mainly focus on the construction of heterogenous catalysts.

1.1 Homogenous Multifunctional catalysts

Although coupling two functional groups is often hard for homogenous catalysts because of their chemical incompatibilities. There are still many examples in this part. One of the most well-known examples of homogenous multifunctional catalysts is enzyme.[3] The spatial poisoning of cooperating functional groups is hindered by enzyme's unique flexible backbone. Despite that, researchers have also successfully prepared many other homogenous catalysts in the last decades. The synthesis of proline-based aminoboronic acids, homoboroproline, has been reported by Whiting et al.[4,5] Homoboroproline exhibited good conversion and high e.e. for enamine-mediated aldol reaction in DMF. Besides, as a commercially available chemical, PBAM can promote the enantioselective synthesis of β-amino-α-bromo nitroalkanes with β-alkyl substituents via homogeneous catalysis,[6] as shown in **Figure 1.1**. In other cases, metal complexes (such as In(III) complexes,[7] Ru(III) complexes[8,9]…) and urea/thiolurea[10,11] showed their bifunctionalities as well. However, the difficulties still lie in the controllable separation between each group. And, similar to regular homogenous catalysts, extra separation steps required at the end of reaction and recyclability are also inevitable issues for this kind of bifunctional catalysts.

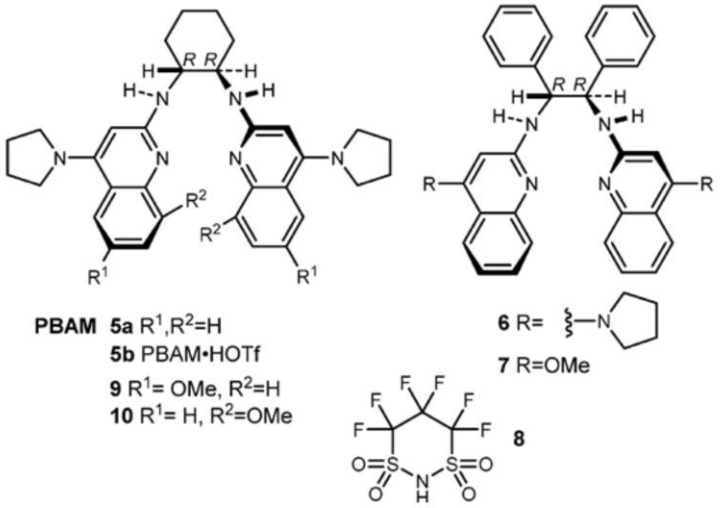

Figure 1.1 Homogeneous acid-base bifunctional chiral organocatalysts, PBAM and its derivatives.[6]

1.2 Heterogeneous Multifunctional catalysts without structural optimized

In the construction of heterogeneous multifunctional catalysts, silica and silica-alumina have been largely employed due to their large surface area and functionalizable sites. One of the simplest ways to obtain multifunctional catalysts has been by immobilizing specific species on those supports by impregnation or chemical-adsorption methods. Corriu et al.[12] and Davis et al.[13] have prepared bifunctionalized heterogeneous catalysts via a "co-polymerization"(or co-condensation) approach. In these cases, tetraethylorthosilicate (TEOS) and different(usually two or more than two) types of organotrialkoxysilane $RSi(OR')_3$, which serve as functional precursors, will be mixed in the presence of a structure-directing regent. It generates a large number of multifunctional and versatile heterogeneous catalysts and allows a well-controlled loading of each groups.[14] In **Figure 1.2**, an acetylacetonate(acac) and thiol groups bifunctionalized SBA-15 can be obtained by the addition of acetylacetonate precursor and thiol precursor during the preparation of this mesoporous organosilica.

Besides, Katz et al.[15] and Corma et al.[16] have reported another more commonly used route which is usually called "post-synthesis". Different from the co-polymerization approach, specific groups will be grafted onto plain support. However, due to several factors like diffusion of each regent through the pore tunnels and residual surface silanol sites, it is hard to control the distribution of functionalized sites directly.[17] Some authors also combined both approaches rather than employed only co-condensation or post synthesis.[18,19,20] Kan et al. have reported such a "hybrid" synthetic route for constructing bifunctional MCM-41. They first prepared a sulfonic acid modified MCM-41 via co-

polymerization approach, then organic amine functional groups were SO_3H-MCM-41 surfaces to gain bifunctional MCM-41, as shown in **Figure 1.3**. This "hybrid" bifunctional MCM-41 exhibited better catalytic activities for one-pot cascade reactions when comparing with bifunctional MCM-41 synthesized via co-condensation method.

The cooperative effect usually improves catalytic performance due to the presence of untethered free silanol groups, the co-exist of different functional groups as well as improved accessibility and stability brought from porous support. However, the poor structuration designation usually causes an absence of shape selectivity and makes those kinds of catalysts hard to avoid the undesired neutralization(quenching) between immobilized basic groups and close acidic sites, which can limit, sometimes, their application in practical reactions.

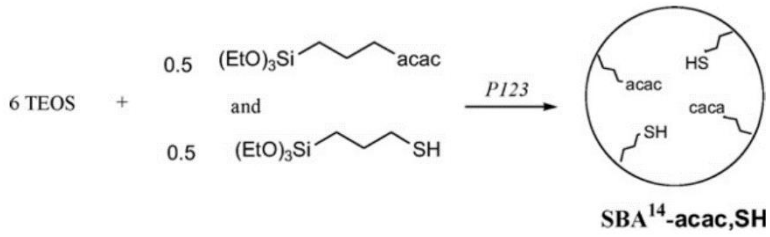

Figure 1.2 Preparation of bifunctional material SBA–acac, SH by co-polymerization.[12]

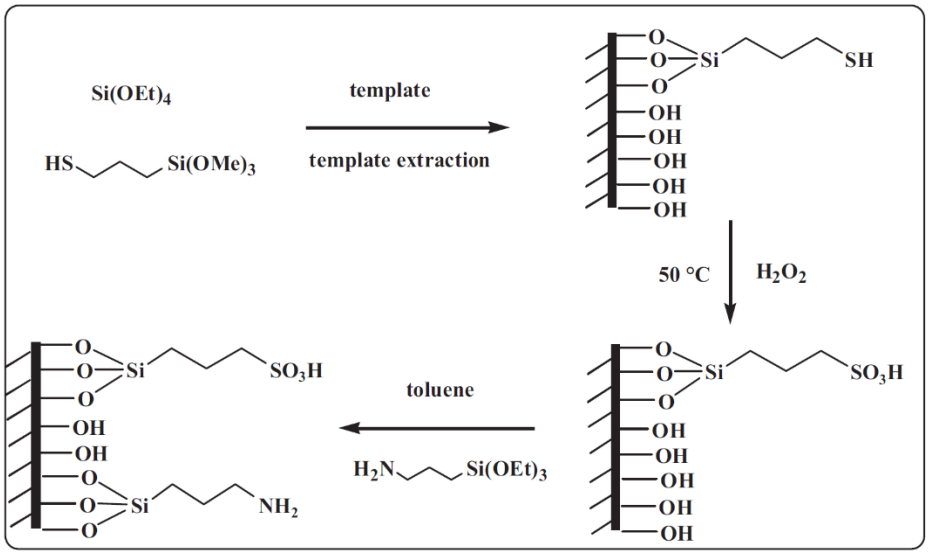

Figure 1.3 Bifunctional material synthesized by utilizing both co-polymerization and post-synthesis methdologies.[20]

1.3 Heterogeneous Multifunctional catalysts with optimized structure

Another important reason for choosing a heterogeneous platform instead of a homogeneous one is to achieve an optimized structure, in other words, spatial separated catalytic functionalities. This may be required to avoid chemical incompatibilities, and it may also be desirable to add directionality to the way the reaction mixture is exposed to the individual catalytic functionalities in tandem catalysis, which are quite hard for homogeneous catalysts since molecules will constantly diffuse in solution.

One strategy is to incorporate one functionality into the framework and another will be immobilized to the surface. During the preparation of Periodic Mesoporous Organosilicas (PMOs), functionalized disilanes are often added as a silica source for the synthesis of supports.[21] Ozin et al. prepared vinyl-ethylene contained bifunctional periodic mesoporous organosilicas(BPMOs) by incorporating bridge-bonded ethylene groups into the frameworks and terminally-bonded vinyl groups on pore channels.[22] Corriu et al.[23,24] have synthesized several optimized structural bifunctional catalysts with their home-made disilanes. They successfully prepared a catalyst that immobilizes amino groups in pore tunnel and sulfonic fragments in its framework. Moreover, materials that compromise chelating groups in frameworks and reactive functional groups in pore channels are also synthesized. Other works with different supports and functionalities are widely reported, showing multiple potential applications of this approach.[25,26,27]

Another methodology to spatial separated catalytic functionalities depends on well-designed structures and optimized synthesis procedures. Yang et al. described the preparation of bifunctional Yolk–Shell Nanoreactors(YSNs) with basic sites located on

the core and acidic on its shell and displayed great performance in Deacetalization–Henry cascade reaction(**Figure 1.4**).[28] Initially, a spherical basic silica core was made and coated with a silica layer. Then sulfonic groups were grafted on the silica layer and this layer was finally selectively etched to create a yolk-shell nanostructure. Song et al. also fabricated an acid-base functionalized core-shell mesoporous silica with acid core and basic shell.[29] Compared with the first approach, structural-design approaches usually avoid the preparation of costly, sophisticated disilane precursors or other specific organic linkers but more works need to be taken into account at the synthesis designing stage.[30,31,32]

Figure 1.4 General procedure for the synthesis of bifunctional Yolk–Shell Nanoreactors with basic sites in the core and thiol groups on the shell.[28]

1.4 Other multifunctional catalysts

Recently, another synthesis methodology has been reported by employing layered silica and use interlayer organic "pillars" to covalently connect each monolayer. The intrinsic lamellar organization enables this class of material for ion-exchange purpose and for obtaining exfoliated and pillared material with multiple catalytic applications.[33]

Corma et al. have successfully synthesized acid-base hybrid materials via one-step hydrothermal process as shown in **Figure 1.5**.[34] They formed isolated aluminosilicate sheets with both amino and sulfonic groups distributed between each individual layers and this material showed good catalytic performance and recyclability as an acid-base bifunctional catalyst for one-pot cascade Deacetalization-Knoevenagel reaction, showing the beneficial cohabitation between acid and base sites.

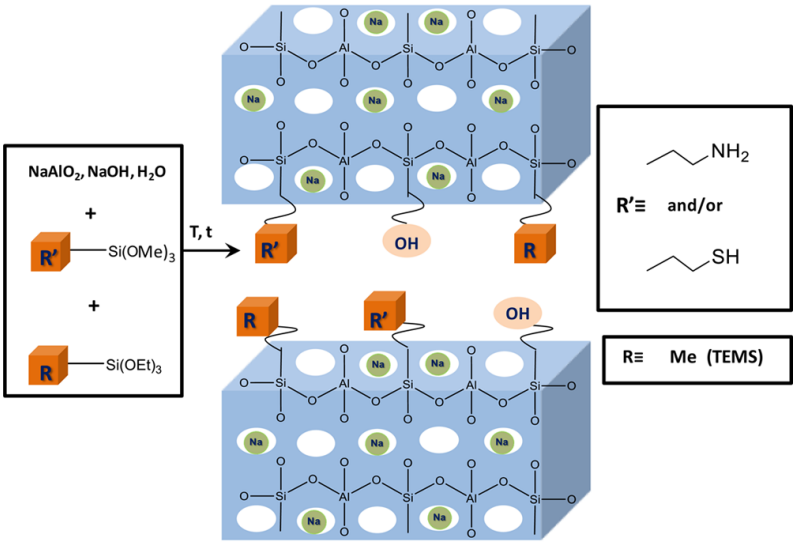

Figure 1.5 General procedure for the synthesis of bifunctional acid−base monolayered hybrid catalysts.[34]

1.5 Mesoporous materials

Mesoporous materials possess the advantages of both microporous and macroporous materials, showing highly hydrothermal and mechanical stability, offering large pore volumes (~1 cm^3/g) and surface areas (~600 m^2/g), and displaying well-defined pore structures with diameters in the 5-20 nm range. This pore structure property is critical to the needs of our proposed work because it affords easy access to large molecules, something that would be much more limited with other crystalline porous materials such as zeolites or metal-organic frameworks (MOFs).

A good number of well-known mesoporous materials can be used for our applications, from which we will choose to start with SBA-15[35] on the account of its simplicity; SBA-15 displays hexagonal one-dimensional pores with well-defined uniform diameters, on the order of a few nanometers. A typical transmission electron microscopy (TEM) image of a SBA-15 solid prepared in our laboratory is shown in **Figure 1.6**. Another advantage of choosing SBA-15 is it can be made in house when the overall synthetic strategy requires the use of the templating agents as blocking elements to prevent deposition inside the pores but also is available commercially. In order to design a universal methodology, the commercial pristine SBA-15 will be selected as support to immobilize functional species in this thesis.

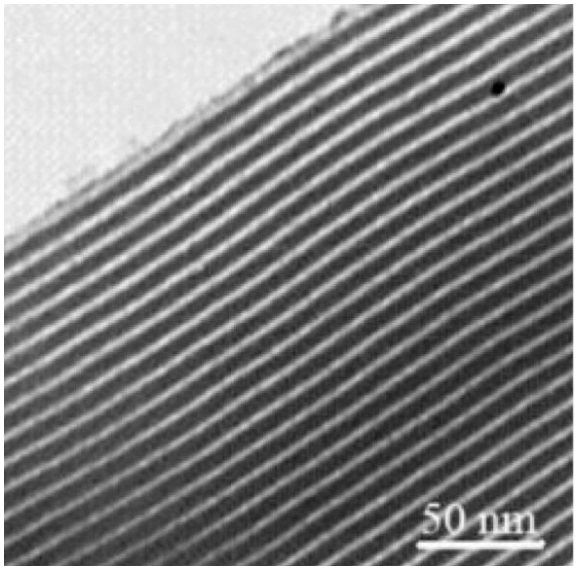

Figure 1.6 Transmission electron microscopy (TEM) images of SBA-15. This image highlights the well-defined nature of the pores in SBA-15. it has a simple hexagonal 1-D structure with parallel pores of about 7 nm in diameter.

1.6 Tethering chemistry

In this thesis, the molecular functionalities will be tethered onto our solid support, SBA15 (a channel-shaped mesoporous silica), to produce all-heterogeneous catalytic systems. The tethering of specific species to surfaces, to oxides in particular, has been greatly facilitated by the development of so-called "click" chemistry in which the desired molecules are attached via the use of an intermediate linking agent. Since silica is used as our support, it provides a large number of surface silanol sites that are capable for chemical anchoring through hydrolysis process. Here, we have honed in on an approach for covalent molecular tethering using well-known alkyltriethoxysilane (R-TEOS) linkers.[36,37,38,39] This is a powerful and versatile procedure, as the functionalized monosilanes can be easily synthesized with many terminal groups, affording multiple ways to add the molecular functionalities of interest to the solid. Our group has also successfully prepared a cinchonidine tethered silica by lab-made cinchonidine functionalized silane as shown in **Figure 1.7**.[40] Moreover, the nature of the catalytic functionality is controllable by changing the length and properties of the link.[38,41,42] For example, Lin et al. have reported that supported organic groups with longer hydrophobic chains, containing alkyl, ureido, or mercapto groups, generate hybrid catalysts with better performance in Henry reaction due to the formation of a surface-bound hydrophobic layer.[43,44] More details of the tethering approach applied will be described in each chapter.

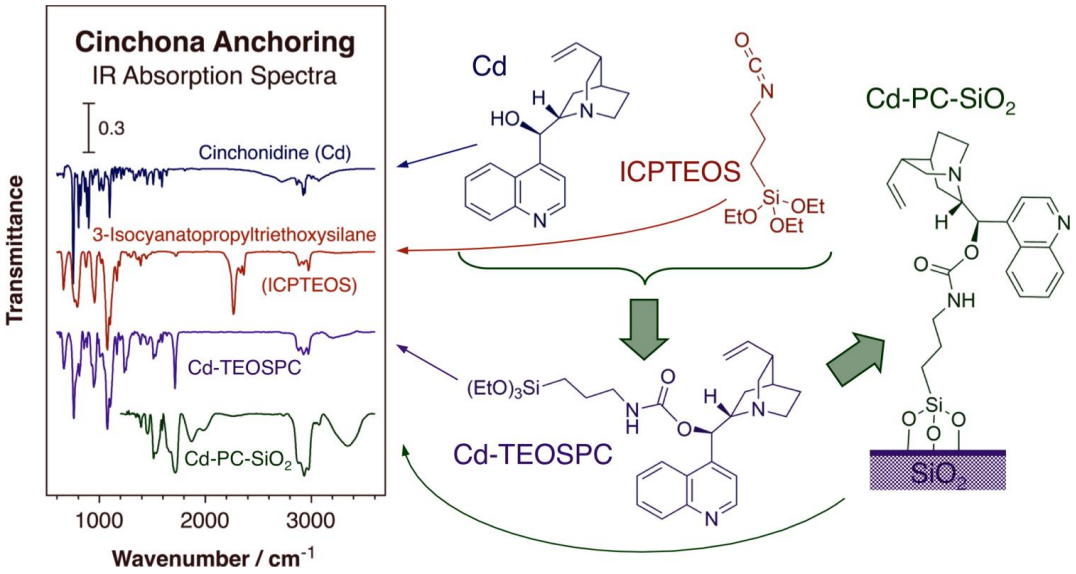

Figure 1.7 Schematic representation of the strategy for the tethering of cinchonidine (Cd) on high-surface-area silica supports.[40]

1.7 Goals for this Thesis

In this thesis, a new approach for constructing acid-base tandem heterogeneous catalyst will be displayed. Those bifunctional catalysts designed should be capable of promoting organic conversions requiring multiple selective steps (i.e. a cascade reaction or domino reaction) in one pot owing to multiple molecular catalytic functionalities anchored. Other advantages for example an easier recycling use are also expected to see due to its heterogeneous character.

What more significant is, this methodology could be further used as a protocol for constructing such tandem catalysts on a silanol-contained platform with spatial isolation since both the Uv/ozonolysis removal process and “click” chemistry accomplished via an R-TEOS link are quite universal strategies, should not be limited to a small range of functional moiety.

References

1. Cozzi, P. G.; Gualandi, A.; Potenti, S.; Calogero, F.; Rodeghiero, G. Asymmetric Reactions Enabled by Cooperative Enantioselective Amino- and Lewis Acid Catalysis; 2020; Vol. 378.

2. Lohr, T. L.; Marks, T. J. Orthogonal Tandem Catalysis. Nat.Chem. 2015, 7, 477−482.

3. P. W. N. M. van Leeuwen, J. C. Chadwick (2011). Homogeneous Catalysts: Activity-Stability - Deactivation. Wiley-VCH, Weinheim.

4. Arnold K., Batsanov A. S., Davies B., Grosjean C., Schütz T., Whiting A. and Zawatzky K., Chem. Commun., 2008, 3879–3881.

5. Georgiou, I.; Whiting, A. Org. Biomol. Chem. 2012, 10 (12), 2422–2430.

6. Stefan F., Meha S., Anthony W., Harald W., Justine R. and Thomas L. , J. Am. Chem. Soc., 2005, 127 , 1206 —1215

7. Li, W.; Xie, J.; Yuan, M.; Zhou, Q. Green Chem. 2014, 16, 4081.

8. Eveline, J.; Jongbloed, L. S.; Tromp, D. S.; Martin, L.; Bas, D. B.; Elsevier, C. J. ChemSusChem 2013, 6, 1737.

9. Georgiou, I.; Whiting, A. Org. Biomol. Chem. 2012, 10 (12), 2422–2430.

10. Weil, T.; Kotke, M.; Kleiner, C. M.; Schreiner, P. R. Org. Lett. 2008, 10 (8), 1513–1516.

11. Sawamura, Y.; Ogura, Y.; Nakatsuji, H.; Sakakura, A.; Ishihara, K. Chem. Commun. 2016, 52 (36), 6068–6071.

12. Mouawia, R.; Mehdi, A.; Reyé, C.; Corriu, R. J. P. J. Mater. Chem. 2008, 18 (35), 4193–4203.

13. Zeidan, R. K.; Davis, M. E. J. Catal. 2007, 247 (2), 379–382.

14. Corriu R. J. P., Embert F., Guari Y., A. Mehdi and C. Reye, Chem.Commun., 2001, 1116.

15. Notestein, J. M.; Katz, A. Chem. - A Eur. J. 2006, 12 (15), 3954–3965.

16. Fuerte, A.; Iglesias, M.; Sánchez, F.; Corma, A. J. Mol. Catal. A Chem. 2004, 211 (1–2), 227–235.

17. Macquarrie D. J., Jackson D. B., Mdoe J. E. J. and Clark J. H., New J. Chem., 1999, 23, 539; Walcarius A. and Delacoˆ te C., Chem. Mater., 2003, 15, 4181.

18. Zhang W.-H., Lu X.-B., Xiu J.-H., Hua Z.-L., Zhang L.-X., Robertson M., Shi J.-L., Yan D.-S. and Holmes J. D., Adv. Funct.Mater., 2004, 14, 544.

19. Mbaraka I. K. and Shanks B. H., J. Catal., 2005, 229, 365.

20. Shang, F.; Sun, J.; Liu, H.; Wang, C.; Guan, J.; Kan, Q. Mater. Res. Bull. 2012, 47 (3), 801–806.

21. Asefa T., MacLachlan M. J., Coombs N. and Ozin G. A., Nature, 1999, 402, 867–871.

22. Asefa, T.; Kruk, M.; MacLachlan, M. J.; Coombs, N.; Grondey, H.; Jaroniec, M.; Ozin, G. A. J. Am. Chem. Soc. 2001, 123 (35), 8520–8530.

23. Zeidan, R. K.; Davis, M. E. J. Catal. 2007, 247 (2), 379–382.

24. Alauzun, J.; Mehdi, A.; Reyé, C.; Corriu, R. J. P. J. Mater. Chem. 2007, 17 (4), 349–356.

25. Kuschel A., Drescher M., Kuschel T. and Polarz S., Chem. Mater., 2010, 22, 1472–1482.

26. Huang, Y.; Xu, S.; Lin, V. S. Y. Angew. Chemie - Int. Ed. 2011, 50 (3), 661–664.

27. Shang, F.; Sun, J.; Wu, S.; Yang, Y.; Kan, Q.; Guan, J. Microporous Mesoporous Mater. 2010, 134 (1–3), 44–50.

28. Yang, Y.; Liu, X.; Li, X.; Zhao, J.; Bai, S.; Liu, J.; Yang, Q. Angew. Chemie 2012, 124 (36), 9298–9302.

29. Li, P.; Cao, C. Y.; Chen, Z.; Liu, H.; Yu, Y.; Song, W. G. Chem. Commun. 2012, 48 (85), 10541–10543.

30. Fujita, S.; Inagaki, S. Chem. Mater. 2008, 20 (3), 891–908.

31. Inagaki, S.; Guan, S.; Ohsuna, T.; Terasaki, O. Nature 2002, 416 (6878), 304–307.

32. Cooper, E. R.; Andrews, C. D.; Wheatley, P. S.; Webb, P. B.; Wormald, P.; Morris, R. E. Nature 2004, 430 (7003), 1012–1016.

33. Ruiz-Hitzky, E.; Darder, M.; Aranda, P. J. Mater. Chem. 2005, 15 (35–36), 3650–3662.

34. Gaona, A.; Díaz, U.; Corma, A. Chem. Mater. 2017, 29 (4), 1599–1612.

35. Zhao D., Feng J., Huo Q., Melosh N., Fredrickson G. H., Chmelka B. F., Stucky G. D Science 279 (1998) 548-552.

36. Kim G.-J., Shin J.-H., Tetrahedron Lett. 40 (1999) 6827-6830.

37. Choong E. S., Annu. Rep. Prog. Chem. C 101 (2005) 143-173.

38. Corma A., Garcia H., Adv. Synth. Catal. 348 (2006) 1391-1412.

39. Kung M. C., Riofski M. V., Missaghi M. N., Kung H. H., Chem. Commun. 50 (2014) 3262-3276.

40. Hong, J.; Lee, I.; Zaera, F. Top. Catal. 2011, 54 (19–20), 1340–1347.

41. Notestein J. M., Katz A., Chem.-Eur. J. 12 (2006) 3954-3965.

42. Copéret C., Basset J.-M., Adv. Synth. Catal.349 (2007) 78-92.

43. S. Huh, H. T. Chen, J. W. Wiench, M. Pruski and V. S. Y. Lin, J. Am. Chem. Soc., 2004, 126, 1010–1011.

44. Tsai, C. H.; Chen, H. T.; Althaus, S. M.; Mao, K.; Kobayashi, T.; Pruski, M.; Lin, V. S. Y. ACS Catal. 2011, 1 (7), 729–732.

Chapter 2: Construction of 1st-Generation Acid-Base Heterogeneous Tandem Catalysts with Amine and Sulfonic Acid

In this chapter, a synthetic procedure was developed to prepare dual acid−base catalysts on a single platform. Mesoporous SBA-15 was derivatized using known grafting chemistry via the following steps:

(1) addition of Boc-protected 3-aminopropyltriethoxysilane;

(2) controlled use of UV/ozonolysis to selectively remove the exterior groups;

(3) decoration of the exterior sites freed in Step 2 with 3-mercaptopropyltriethoxysilane;

(4) selective oxidation of the mercaptan groups to sulfonic acid;

(5) pyrolytic deprotection of the amine.

The resulting catalysts contain sulfonic acid functionality on the external surfaces and entrance of the pores and amino groups deep inside those pores, at coverage ratios that can be controlled by tuning the exposure time during the UV/ozonolysis step. The samples were fully characterized by ^{13}C and ^{29}Si solid-state NMR, infrared absorption spectroscopy, acid−base titrations, and N_2 adsorption isotherms measurements, and they were successfully tested for the promotion of a cascade Henry reaction. Optimum performance was seen with the catalyst having an overall 1:2 acid: base molar ratio.

2.1 Introduction

The design of tandem catalyst applied in a cascade process is attracting people's interest since such a combined system could significantly reduce the reactor required, even if that synthesis requires multiple steps. Such reduced systems also lead to a less the number of isolation and purification steps required.[1] In other words, Those reduced steps could lead to a large save in energy which is mostly due to the elimination of extra heat-based processing such as evaporation, distillation, recrystallization, etc. A huge reduction in waste generation, which mostly comes from the extra solvent used during those separation steps, will be found this way. Unfortunately, combining catalytic functionalities such as acids and bases in solution is often limited by chemical incompatibilities between the functional components.

A couple of strategies can be followed to prevent chemical incompatibility. First of all, mechanical control is a good way to physically separate incompatible components in each step.[2,3] With specifically designated equipment, such as specific flow designs and physically separated catalysts, incompatible components will undergo their specific step individually(i.e. different time and temperature) and sequentially.[2,3] However, one of the drawbacks of this approach is the transfer issues for some unstable intermediates from one step to the next step. Besides, our group has also found amine-derivatized titania nanoparticles deactivate separate Au/TiO_2 catalysts if both are mixed in the same solution, which suggests solid catalysts may still interfere with each other. Second is to design a cascade reaction process, in which at least two consecutive reactions are performed without the need for isolation.[4,5] In this way, catalysts need to be chosen orthogonal to each

step to minimize by-product.[6–9] This is a valuable approach, but it is one that is somewhat restrictive and that may not be implementable in some cases, especially if specific selective and irreplaceable steps are required in complex synthetic schemes.

Third, the Construction of heterogeneous tandem catalysts the creation of heterogeneous systems seems to be a better approach. It maintains the functionalities of each individual catalytic motifs by spatial separation. Reported examples of this approach include the selective construction of polymer scaffolds with variable catalytic functionalities,[9] the attachment of catalysts to resins[10] or multi-functional grafting to Cellulose nanocrystals (CNCs).[11] There are many recent citations of heterogeneous tandem and cascade catalysis in the literature that follow this third approach, many involving acid−base combined chemistry.[1,12–26] Choosing good support with both good stability and high surface area is important in this case. The other problem is the difficulty in designing heterogeneous tandem catalysts synthetic strategy due to the incompatibility of each moiety. Literature mentioned above have reported different and interesting synthetic methodologies for the addition of the several desired functionalities to a porous solid, but they do not yet offer a universal protocol for doing this. In addition, most of them show a randomly-distributed functionalities and only a handful of them address the issue of the spatial isolation of the different added groups, an important consideration when dealing with cascade processes involving unstable intermediates.[27–31] It is desirable to expand the library of synthetic routes by which such multifunctional catalysts can be made.

In this chapter, we will introduce a novel methodology that relies on known grafting chemistry to add molecular structures to solid surfaces and a combined ultraviolet-

radiation/ozonolysis treatment for the controlled and selective removal of some of the tethered functionalities in specific regions of the solid. The resulting catalysts were thoroughly characterized to corroborate the success of the synthetic approach, and their catalytic performances were tested for a prototypical Henry conversion. The details of this work follow.

Only my part of data will be shown in this thesis and the rest of them can be found in the publishment mentioned in acknowledgment.

2.2 Experimental Details

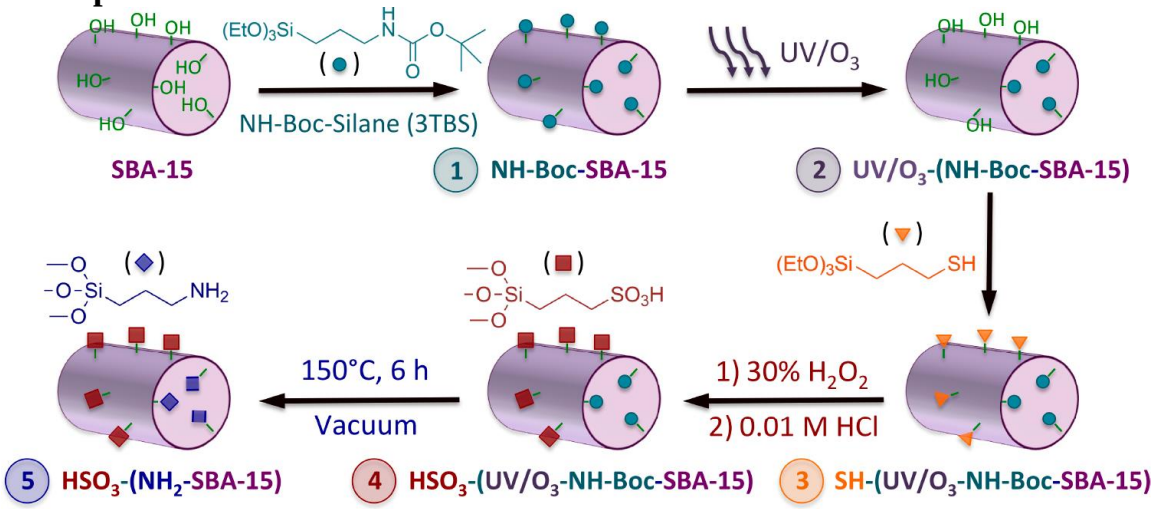

Figure 2.1 Synthetic strategy used in this research for the making of dual acid−base catalysts.

Most of the chemicals used, including the SBA-15, were purchased from Sigma-Aldrich (research purity) and used as supplied.

Both acidic (sulfonic acid) and basic (amine) moieties were tethered to SBA-15 mesoporous support[40] according to the procedure. shown in **Figure 2.1**, relying on well-known grafting chemistry based on alkyltrialkoxysilane linkers.[33−35,38−44] The synthetic steps were the following:

1. Tethering of 3TBS to the surfaces of SBA-15 (Step 1, to make **NH-Boc-SBA-15**): SBA-15 (1 g) was calcined under vacuum at 200 °C for 2 h, after which 25 mL of anhydrous toluene and 0.5 g of 3-tert-Butyloxycarbonylaminopropyltriethoxysilane (**3TBS**) were introduced into the flask. The condensation was conducted under a nitrogen atmosphere at 110°C for 48 h, and it was followed by filtering, washing with toluene, and drying under vacuum overnight.

2. Selective removal of −NH-Boc groups from the outside and pore-entrance surfaces (Step 2, to make **UV/O_3-(NH-Boc-SBA-15)**):

The **NH-Boc-SBA-15** samples were exposed to a combination of ultraviolet (UV) radiation and ozone for various hours (**typically 3 h, unless otherwise indicated**), using a Spectrolinker XL-1500 UV cross-linker instrument equipped with both its original λ (wavelength) = 254 nm lamp and an additional λ = 185 nm radiation source (to produce ozone from molecular oxygen).[42,43] The UV power was set to 10 000 μW/cm^2.

3. Tethering of −SH groups to the outside and pore entrance surfaces (Step 3, to make **SH-(UV/O_3 NHBoc-SBA-15)**):

3-Mercaptopropyltriethoxysilane (0.1 g) was mixed with 0.3 g of **UV/O_3-(NH-Boc-SBA-15)** under a nitrogen atmosphere for 24 h at 80 °C. The resulting solid was collected by filtering, and washed with toluene, and dried under vacuum overnight. Again, an excess of 3-mercaptopropyltriethoxysilane was used to ensure the derivatization of all newly freed silanol groups.

4. Oxidation of −SH groups in **SH-(UV/O_3-NH-Boc-SBA-15)** to −HSO_3 (Step 4, to make **HSO_3-(UV/O_3-NHBoc-SBA-15)**):

0.3 g of **SH-(UV/O_3-NH-Boc-SBA-15)** was stirred in 10 mL of a 30 wt % H_2O_2 aqueous solution at room temperature in air for 24 h. The solid was filtered and washed several times with deionized water, and the resulting solid was added to a 50 mL 0.01 M HCl solution for 12 h. The solid product was collected by filtering, washed with deionized water until the pH value of the filtrate reached a value close to 7, and dried overnight under vacuum.

5. Deprotection of $-NH_2$ groups in **HSO_3-(UV/O_3-NHBoc-SBA-15)** (Step 5, to make the final **HSO_3-(NH_2-SBA-15)**):

The carbamate deprotection was performed by thermal treatment of HSO3-(UV/O3-NH-Boc-SBA-15) at 150 °C under vacuum for 6 h.

Synthesis of 3-tert-butyloxycarbonylaminopropyltriethoxysilane (**3TBS**):

3-aminopropyltriethoxysilane (3.1 g, 14.2 mmol) and di-tert-butyl dicarbonate (3.5 g, 15.9 mmol) mixed in 12 mL of ethanol with stirring overnight at room temperature. After that, the solvent is removed under vacuum, and the residual liquid is distilled to afford 3TBS as a colorless liquid.

The ^{29}Si and ^{13}C cross-polarization magic-angle spinning (CP/MAS) NMR data were acquired on a Bruker Avance 600 spectrometer equipped with a 4 mm H/X CP-MAS probe operating at 119.2 MHz. All spectra were recorded employing a spinning speed of 10 kHz. For the ^{29}Si CP/ MAS NMR spectra, a cross-polarization contact time of 2 ms, a ^{1}H decoupling bandwidth of 80 kHz, and a recycle time of 3s were used. Data were acquired as 12000 coadded 2048 complex data point FIDs with a 100 kHz sweep width. Post-acquisition processing consisted of exponential multiplication with 200 Hz of line broadening and zero filling to 4096 data points. Chemical shifts were referenced to an external DSS sample.

Infrared absorption (IR) spectra were acquired in transmission mode using a Bruker Tensor 27 Fourier-transform infrared (FTIR) spectrometer.

The surface concentrations of the sulfonic acid and amine groups were quantified by acid−base back-titrations. The amine coverages were estimated by neutralizing the

catalysts (25 mg) with HCl solution (5 mL, 0.0224 M), filtering the solid and quantitative collecting the solution, and titrating the filtrate with a NaOH solution (0.01 M), using phenolphthalein as the indicator. The acidic groups were estimated by first reacting the solid with a known excess of Na_2CO_3 (4 mL, 0.01M solution) and treating the filtered solution with a fixed excess of HCl (5 mL, 0.0244 M solution) before titrating with NaOH (0.01 M), again using phenolphthalein as the indicator.

The surface areas, pore volumes, and pore size distributions were estimated from N_2 adsorption−desorption isotherms obtained using a commercial 2000e Model 25 Nova Win vacuum volumetric gas sorption system. The data were analyzed by using the Barrett−Joyner−Halenda (BJH) isotherm equations on desorption branches of the data.

The catalytic reactions were carried out as follows: the catalyst (25 mg) was first heated at 50 °C for 2 h under vacuum to remove any absorbed water. Nitromethane (4 mL) and benzaldehyde dimethyl acetal (0.25 mmol) were added under a nitrogen atmosphere, and the mixture was stirred at 90 °C, still under nitrogen. Aliquots (0.1 mL) were taken at different time intervals to monitor the reaction progress; they were analyzed by gas chromatography, using a HP-50 column, to determine the yields of benzaldehyde and β-nitrostyrene (2-nitrovinylbenzene).

2.3 Catalyst Characterization: ^{13}C CP/MAS NMR

The integrity of the tethered organic moieties should be checked with ^{13}C CP/MAS NMR and IR. However, this part of work is mostly accomplished by Dr. Zhihuan Weng. The only ^{13}C NMR spectra I have is for the final synthesized catalyst in Step 5: **HSO_3-(NH_2-SBA-15**), as shown in **Figure 2.2.** The peak assignments are straightforward[17,32,36] and the presence of **-HSO_3** and **-NH_2** moieties are clearly indicated by peaks at 53 ppm(-**C**H_2-HSO_3) and 42 ppm(-**C**H_2-NH_2), respectively. Besides, no signal for the main peaks associated with the Boc protecting group, namely, the signal at 158 ppm for the carboxylic group of the amido link and those for the tert-butyl group at 27 and 79 ppm can be observed in this spectra, complying with the leaving of Boc group during the deprotection process in Step 5.

However, more detailed information including samples in the other steps and the pure, untethered NH-Boc-silane precursor, which gives a better proof for overall grafting work, are included in our previous publishment mentioned in acknowledgment.

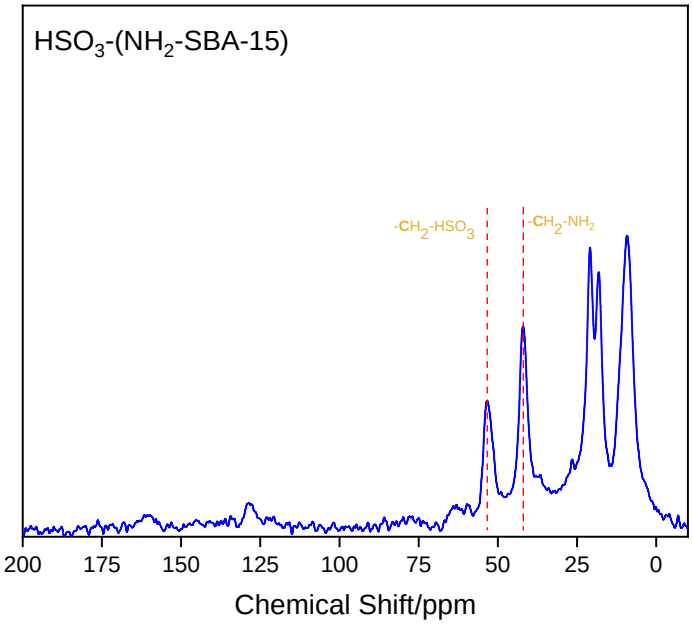

Figure 2.2 ^{13}C CP/MAS NMR spectra for synthesized catalyst: HSO_3-(NH_2-SBA-15).

2.4 Catalyst Characterization: IR

Further information on the nature of the tethered species was obtained by using IR spectroscopy. Same with ^{13}C NMR, I will only report those data achieved by myself. Another IR spectroscopy for studying the effect of the UV/ozonolysis treatment is shown in our previous publishment.

The resulting data for each key synthetic step during the making of the **HSO_3-(NH_2-SBA-15)** are shown in **Figure 2.3**. In **Figure 2.3**, several peaks can be seen associated with the tethered functionalities, among which those associated with the Boc protecting group are the most prominent. In **Figure 2.3**, due to the carboxylic group of Boc group(as circled), we are able to observe a broad peak band at about 1700 cm^{-1}, but also evident are the features at 1371 and 1398 cm^{-1} due to the symmetric deformation vibrations of the terminal methyl groups. All those signals disappear once the samples are heated in vacuum to remove the deprotection group as shown in the top green trace, as expected. Because of the prominence of the Boc peaks in the IR spectra, this technique is ideal to study the effect of the UV/ozonolysis treatment on our catalysts.

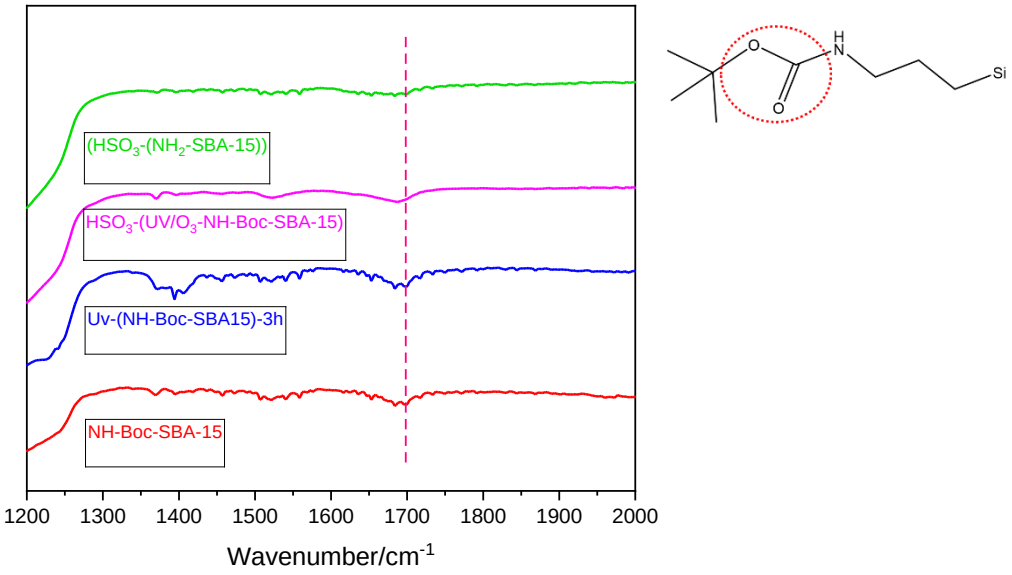

Figure 2.3 Transmission infrared absorption (IR) spectra from the solid samples obtained after key steps of the synthesis of our catalysts.

2.5 Catalyst Characterization: ^{29}Si CP/MAS NMR and Acid−Base Titrations

Functional moiety tethering and Uv/ozonolysis removal process (Steps 1 and 3) were checked by using ^{29}Si CP/MAS NMR. In meanwhile, the preservation of the tethered groups throughout the rest of the synthetic process and the efficiency of each step can be also evaluated via this analysis. Pristine **SBA-15** support and typical spectra obtained after each step are reported in **Figure 2.4**. For the spectra of Pristine **SBA-15,** only Q peak, which is relative to the signals from the nonderivatized Si−OH groups can be observed. Then for ^{29}Si solid state NMR spectra of all functionalized SBA-15, T peaks, the signal from the tethered species, can be found at the range of -40 to -70 ppm. Specifically, the peak pattern can be well-assigned according to what has been reported previously for similar systems.[44–46] Six major signals at -92, -102, and -112 ppm, corresponding to Q^2, Q^3, and Q^4 species, and at -47, -57ppm, and -67ppm, corresponding to T^1 ($RSi(OSi)(OH)_2$, where R refers to tethered functional groups), T^2 ($RSi(OSi)_2(OH)$) sites, and T^3 ($RSi(OSi)_3$), respectively, can be observed in **Figure 2.4.** The peaks in those data not only confirmed the existence of the tethered species on the surface of the SBA-15 pores but also provide information about the type of bonding involved.

The resulting T and Q peaks are integrated and the area percentages of T peak for each key step are shown in **Table 2.1.** Besides, acidic($-HSO_3$) or basic($-NH_2$) moieties contents are determined via acid−base titrations, also as shown in **Table 2.1.** It can be seen that a significant fraction of silanol (Si−OH) groups in SBA-15, around 30%, are consumed during the tethering of the Boc-protected amine groups in the first step (%T in this table indicates the percentage peak area value of **T/(T+Q)**). Incomplete consumption of

silanol groups is expected, as it is known that only about half of the terminal silanol groups are available on the surface for reaction.[47] It is also evident from the ^{29}Si CP/MAS NMR data that bonding to the surface can occur via one, two, or three Si−O−Si links, but that the dominant modality (which is shown as the most major peak) is with two bonds. This is also common, and has been seen in other cases.[33−35,44,45,48]

Surprisingly, a more interesting trend is found in **Table 2.1.** : the ^{29}Si CP/MAS NMR signals follow and provide a semiquantitative measure for, the addition or elimination of surface tethered groups after each step of the synthesis. As we discussed in the last paragraph, the %T suggests a percentage of the surface silanol coverages. The %T from ^{29}Si NMR and titration data agreed quite well for the samples with the addition or removal of acid/base sites. Especially for the trend of moiety addition or removal we assumed from procedure, the increase or decrease %T complied with each step quite well. For example, in Step 2, about a third of NBoc groups were removed from titration data, resulting in a loss %T for also around 30%, indicating functional groups detachment by ozonolysis. An increase of %T is observed after Step 3, for SH-(UV/O3-NH-Boc-SBA-15) upon the addition of the thiol units. **HSO_3-(UV/O_3-NH-Boc-SBA-15)** in Step 4, after thiol oxidation, shows a decrease again by about a quarter. This may indicate a slight moieties removal from SBA-15 surface caused by thiol oxidation/hydrolysis step. One note of caution is warranted here: because the signal in CP/MAS NMR relies on polarization transfer from hydrogen atoms to the atoms being probed, which will be highly affected by the mass of sample being analyzed, the technique is in general not quantitative; the analysis provided in **Table 2.1** should therefore be taken with a grain of salt. Nevertheless, a similar

analysis has been used in the past successfully for the characterization of different types of silica and aluminosilicate samples.[44,49] Also, our analysis relies on relative signal intensities, which minimizes some of the problems associated with CP/MAS NMR data quantitation.

Finally, titration experiments indicate a 1:2 acid: base ratio in the final sample for this case. That ratio can be tuned by varying the time of UV/O_3 exposure in Step 2.

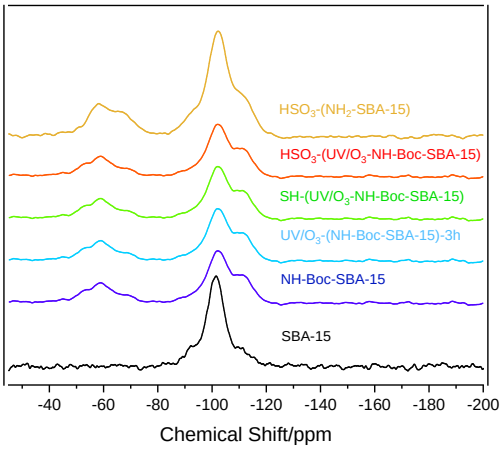

Figure 2.4 ^{29}Si cross-polarization magic-angle-spinning (CP/MAS) NMR spectra for our SBA-15-based catalysts after each synthetic step, as indicated in **Figure 2.1**

Table 2.1 ^{29}Si CP/MAS NMR Peak Areas from **Figure 2.4** and Surface Coverages of Acidic and Basic Sites, Measured by Titration Experiments, for Samples Obtained after Each Step of the Catalyst Synthesis, as Indicated in **Figure 2.1**

[a] This intermediate product has **not** been tested for titration experiments.

Sample	%T	Acid content/ mmol g^{-1}	base content/ mmol g^{-1}	Total sites content mmol g^{-1}
SBA-15	0	N/A	N/A	N/A
NH-Boc-SBA-15	29	N/A	0.32	0.32
UV/O_3-(NH-Boc-SBA-15)-3h	20	N/A	0.21	0.21
SH-(UV/O_3-NH-Boc-SBA-15)[a]	31	N/A	N/A	N/A
HSO_3-(UV/O_3-NH-Boc-SBA-15)	24	0.10	N/A	N/A
HSO_3-(NH_2-SBA-15)	28	0.10	0.18	0.28

2.6 Catalyst Characterization: N_2 Adsorption Isotherms

Texture properties were further characterized by recording N_2 adsorption-desorption isotherms. Thanks to the well-defined structure of the pores in mesoporous materials such as SBA-15, the pore diameter distributions can be used to detect substitutions on the surfaces of such pores. Additional data can be extracted in terms of total surface area and pore volume as well.

Thanks to the good stability of SBA-15, all samples show a Barrett−Joyner−Halenda (BJH) type IV isotherm behavior with a H1 hysteresis loop which is typically observed for SBA-15, as is also characteristic of ordered mesoporous materials.[50,51] It indicates a well-maintained intrinsic mesoporous structure for SBA-15 support during the overall synthetic strategy. Pore size distributions obtained from desorption branch are displayed in **Figure 2.5** and detailed results are summarized in **Table 2.2**.

It can be seen that in Step 1, there are significant losses of area and pore volume upon the initial tethering of the Boc-protected amine groups, and the average pore diameter is reduced by approximately 1 nm, suggesting a successfully grafting work for such buck groups. Then both surface area and the average pore diameter increase upon UV/O_3 treatment (Step 2), as some of the tethered material is removed, decrease again upon the addition of the acidic functionality (Step 4). Those values finally go up again as the Boc-protecting groups are removed from the amine moieties (Step 5). However, the changes are in general not as marked in the pore volume, possibly because of well-preserved inner pore sites during UV/ozonolysis treatment in Step 2, but a significant volume increase is

nevertheless seen once those (bulky) Boc groups located inside the pore tunnel, are removed in the deprotection step.

Last, for the pore size distribution in **Figure 2.5,** it is also worth pointing out that the narrow distribution of the pore diameter in SBA-15 is retained for all stages except for our final product **HSO_3-(NH_2-SBA-15)** as shown in the blue trace. This relatively wider pore size range is a "primary" **bimodal pore size distribution** resulting from HSO_3- grafted pore entrance part, which may lead to smaller pore size and a well-retained NH_2- grafted pore inner pore, larger pore size can be assigned to. Such a bimodal pore size distribution will be much clearer to observe and further studied in Chapter 3 for the case of 2nd-generation tandem catalyst, where two functional moieties with more size difference will be introduced.

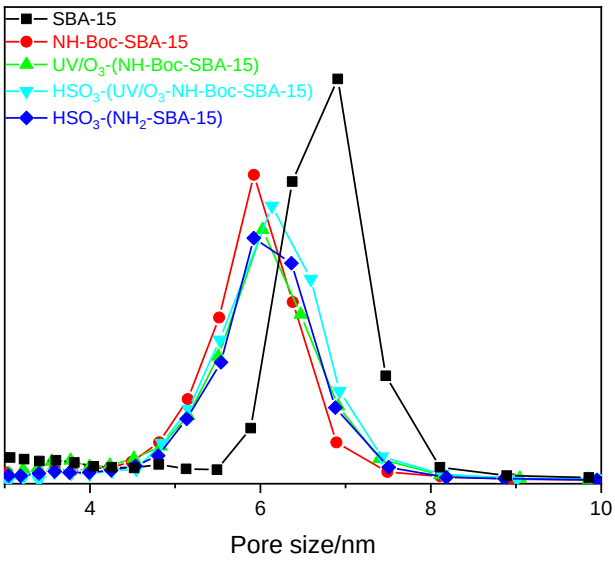

Figure 2.5 Pore size distributions from N_2 adsorption-desorption isotherms for our SBA 15-based catalysts after each synthetic step, as indicated in **Figure 2.1**.

Table 2.2 N_2 Adsorption Isotherms Data Summary
[a] V_T = total pore volume
[b] Calculated using the Barrett–Joyner–Halenda (BJH) equation on the desorption branch.

Step	Sample	Surface area/m^2g^{-1}	V_T/ cm^3 g^{-1}[a]	Pore size/nm[b]
0	SBA-15	787	1.11	6.90
1	NH-Boc-SBA-15	439	0.69	5.92
2	UV/O_3-(NH-Boc-SBA-15)	471	0.69	6.03
4	HSO_3-(UV/O_3-NH-Boc-SBA-15)	397	0.70	5.92
5	HSO_3-(NH_2-SBA-15)	475	0.78	6.13&6.38

2.7 Catalytic Performance

The dual **HSO_3-(NH_2-SBA-15)** acid−base catalysts made by our synthetic procedure were tested for the two-step conversion of benzaldehyde dimethyl acetal to β-nitrostyrene, following an initial acid-catalyzed Deacetalization reaction to produce benzaldehyde and a subsequent addition of nitromethane via a base-catalyzed Henry reaction. This process, shown at the top of **Table 2.3**, has been often used as a prototypical probe for cascade acid-base catalysis.[28,52−54] Our first task here was to make sure that both acidic and basic functionalities are necessary. The blank experiments with pure SBA-15 were performed in the first entry for both **Table 2.3** (Deacetalization) and **Table 2.4** (Henry reaction). Very poor conversion indicates SBA-15 support itself cannot promote either step of the reaction.

Then the conversion of benzaldehyde dimethyl acetal + nitromethane mixtures(acid step) and benzaldehyde + nitromethane mixtures(base step) were both tested with mono-functionalized catalysts: Boc-unprotected **(NH_2-SBA-15)** amine groups, and sulfonic acid **(HSO_3-SBA-15)** (entries 2 and 3 in **Table 2.3** and **2.4**, respectively). Clearly, none of those catalysts promote the complete conversion to β-nitrostyrene: the amine-based catalysts cannot convert the dimethyl acetal reactant at all, and the sulfonic acid catalyst is quite efficient in promoting the first step, to benzaldehyde, but cannot help with the nitromethane addition. Only the catalyst containing both acidic and basic sites is capable of carrying out the conversion to completion (**Table 2.3**, entry 4). Third, we did not see any evidence for the need for close acid−base cooperative activity, as reported for related coupling systems.[55] Anyway, such a cooperative activity did be found in our 2nd-

generation cinchonidine-phosphonic tandem catalyst in Chapter 3 due to different system constructed and we will discuss it later.

Next, the performance of the catalyst can be optimized in terms of tuning the ratio of acidic (HSO_3−) to basic (NH_2−) sites present on the surface. Those part of work was mostly accomplished by Dr. Zhihuan and won't be included in this thesis.

Table 2.5 summarized my part of work for performance optimization. Different from regular catalyst made via a 3-hour Uv/O_3 treatment, catalyst in entry 2 and entry 4 took 2 hours and one day(24 hours) instead, respectively. Similar to catalysts in entry 5, 3 times of NH-Boc precursor were added during the initial tethering step in Step 1, which result in a larger initial NH_2- contents. As shown in **Table 2.5,** shorter exposures (entry 2) or a larger initial NH_2- contents (entry 5) result in catalysts with an insufficient concentration of acidic sites, making the conversion of the first step slow: the catalyst made with 2 h UV/O_3 exposure only convert 31% of reactant in 1h. And the one with larger initial NH_2- contents performed worse, with a conversion of 15% for the same time. Long exposures (entry 4), by contrast, remove most of the basic sites, so the resulting catalysts have enough acidic sites to rapidly convert all the initial benzaldehyde dimethyl acetal to benzaldehyde, but not to the final product; virtually no β-nitrostyrene was detected in the case with as long as 24 hours treatment. Due to the lack of benzaldehyde produced in Deacetalization, which serves as reactant for henry reaction, entry 2 shows less than a half β-nitrostyrene yield compared with catalyst with 3 h UV/O_3 exposure in entry 3. Thanks to high catalysis activity for henry step, entry 5 did indicate a similar yield with entry 3. However, three times NH-Boc precursors were used for this entry which

generates more waste than the original approach. So even if with a similar yield, the regular **HSO_3-(NH_2-SBA-15)** with 3h Uv/Ozonolysis is still our best choice.

A comparison of the performance of the optimized bifunctional catalyst against a physical mixture of two catalysts with acid-only **(HSO_3-SBA-15)** and base-only **(NH_2-SBA-15)** sites, respectively, is displayed in entry 3 and entry 6 in **Table 2.5.** It can be seen that the physical mixture is more active in terms of overall conversion (almost twice) but significantly less selective toward the final product than the bifunctional catalyst, which finally results in a less β-nitrostyrene yield, in spite of the fact that the total number of both acid and base sites were matched by adjusting the masses of the two catalysts used in the former case. In this particular case, the performance of the bifunctional catalyst is preferred because of its significantly better selectivity, which may due to our spatial separated and well-ordered acidic and basic sites.

In the part of work done by Dr. **Zhihuan,** he calculated reaction rate constants of k_1 = 1 H-mmol^{-1} min^{-1} and k_2 = 30 NH_2-mmol^{-1} min^{-1}, respectively. He further highlighted the fact that although the second step is intrinsically much faster than the first, more basic than acidic sites are needed because the steady-state concentration of the intermediate (benzaldehyde) is always low.

The recyclability of the catalysts was tested by Dr. **Zhihuan**. A loss of approximately 5% in total activity is seen by the third run, without any noticeable loss in selectivity. The silane-based bonds used for tethering are quite robust and the propyl amino and sulfonic acid groups are also fairly stable, but other factors may play a role in this subtle loss in activity.

Table 2.3 Deacetalization reaction. Starting from benzaldehyde dimethyl acetal and solvent. Used To Test Our Acid−Base Dual Catalysts and Performance versus Reference Monofunctional Acidic or Basic Catalysts.

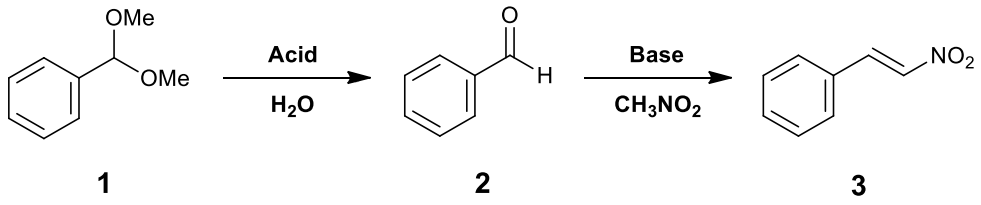

entry	catalyst	Time/h	Conversion%	Yield of **2%**	Yield of **3%**
1	SBA-15	12	7	7	0
2	NH_2-SBA-15	16	0	-	-
3	HSO_3-SBA-15	2	99.1	99.1	0
4	HSO_3-(NH_2-SBA-15)	13	98.7	0.3	98.4

Table 2.4 Henry Reaction. Starting from benzaldehyde and nitromethane. Used To Test Our Acid−Base Dual Catalysts and Performance versus Reference Monofunctional Acidic or Basic Catalysts.

Entry	catalyst	Time/h	Yield of **3%**
1	SBA-15	12	0
2	NH_2-SBA-15	1	96.4
3	HSO_3-SBA-15	12	0

Table 2.5 Optimization Tests for Our Dual Acid−Base Catalysts in the Deacetylation Plus Henry Cascade Reaction Sequence. The results in 1h are shown in the **figure** below the table for comparison.

entry	catalyst	Time/h	Conversion%	Yield of **2%**	Yield of **3%**
1	HSO_3-(3h UV/O_3-NH_2-SBA-15)	13	98.7	0.3	98.4
2	HSO_3-(2h UV/O_3-NH_2-SBA-15)	1	31.6	26.6	5.0
3	HSO_3-(3h UV/O_3-NH_2-SBA-15)	1	40.2	28.1	12.1
4	HSO_3-(24h UV/O_3-NH_2-SBA-15)	1	72	72	-
5	HSO_3-(3h UV/O_3-3NH_2-SBA-15)	1	15.6	3.4	12.2
6	HSO_3-SBA-15 +NH_2-SBA-15	1	61.5	50.0	11.5

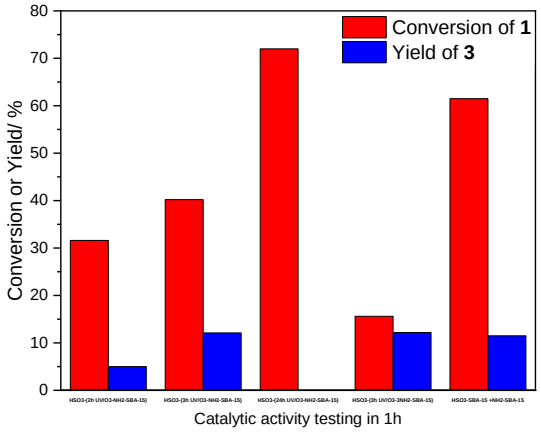

2.8 Conclusion

A new promising synthetic strategy is reported for the construction of solid catalysts with dual molecular functionality, specifically in this chapter, with sulfonic acid and amine groups, to act as acidic and basic sites, respectively. Our approach relies on: (1) the use of well-known grafting chemistry to tether molecular moieties to oxide surfaces via alkyltri-alkoxysilane (R-TEOS) linkers; (2) the implementation of combined ultraviolet light plus ozonolysis treatments for the controlled partial removal of tethered fragments from the surface; and (3) the use of protecting groups to avoid reactions between incompatible functionalities, in this case, the acidic and basic groups. Solid-state NMR and infrared absorption spectroscopies were combined with acid−base titrations and N_2 adsorption isotherm measurements to fully characterize and corroborate the success of each of the steps associated with this synthesis. The components were assembled together in a five-step protocol to prepare specific tandem sulfonic acid-amine derivatized SBA-15 mesoporous materials, but the procedure is fairly general and could be adapted for the synthesis of other dual catalysts.

By tuning UV/ ozonolysis exposure length, the overall ratio of the coverages of the two functionalities on the surface can be optimized for reaction. Even if most works in this optimization are done by Dr. **Zhihuan**, **HSO_3-(3h UV/O_3-NH_2-SBA-15)** can still be found to have the best performance among all catalysts prepared. Another key advantage of our approach is that the UV/ ozonolysis treatment provides the means for the spatial separation of the acidic and basic sites, with the former placed on the outside surfaces and the front of the pores and the latter located deeper inside those pores. This spatial isolation might be

one reason for the better catalytic activity than its physical mixture. Finally, thanks to tests performed by Dr. **Zhihuan**, the optimized catalyst could be recycled, although a slow deterioration of its performance, namely, a drop of ~5% in total activity, was seen after three cycles.

References

1. Lohr, T. L.; Marks, T. J. Orthogonal Tandem Catalysis. Nat. Chem. 2015, 7, 477−482.

2. Tietze, L. F. Domino Reactions in Organic Synthesis. Chem. Rev.1996, 96, 115−136.

3. Nicolaou, K. C.; Montagnon, T.; Snyder, S. A. Tandem Reactions, Cascade Sequences, and Biomimetic Strategies in Total Synthesis. Chem. Commun. 2003, 551−564.

4. Snead, D. R.; Jamison, T. F. A Three-Minute Synthesis and Purification of Ibuprofen: Pushing the Limits of Continuous-Flow Processing. Angew. Chem., Int. Ed. 2015, 54, 983−987.

5. Tsubogo, T.; Oyamada, H.; Kobayashi, S. Multistep Continuous-Flow Synthesis of (R)- and (S)-Rolipram Using Heterogeneous Catalysts. Nature 2015, 520, 329−332.

6. Bruggink, A.; Schoevaart, R.; Kieboom, T. Concepts of Nature in Organic Synthesis: Cascade Catalysis and Multistep Conversions in Concert. Org. Process Res. Dev. 2003, 7, 622−640.

7. Fogg, D. E.; dos Santos, E. N. Tandem Catalysis: A Taxonomy and Illustrative Review. Coord. Chem. Rev. 2004, 248, 2365−2379.

8. Wasilke, J.-C.; Obrey, S. J.; Baker, R. T.; Bazan, G. C. Concurrent Tandem Catalysis. Chem. Rev. 2005, 105, 1001−1020.

9. Lu, J.; Dimroth, J.; Weck, M. Compartmentalization of Incompatible Catalytic Transformations for Tandem Catalysis. J. Am.Chem. Soc. 2015, 137, 12984−12989.

10. Phan, N. T. S.; Gill, C. S.; Nguyen, J. V.; Zhang, Z. J.; Jones, C. W. Expanding the Utility of One-Pot Multistep Reaction Networks through Compartmentation and Recovery of the Catalyst. Angew.Chem., Int. Ed. 2006, 45, 2209−2212.

11. Ellebracht, N. C.; Jones, C. W. ACS Catal. 2019, 9 (4), 3266–3277.

12. Huang, Y.; Trewyn, B. G.; Chen, H.-T.; Lin, V. S. Y. One-Pot Reaction Cascades Catalyzed by Base- and Acid-Functionalized Mesoporous Silica Nanoparticles. New J. Chem. 2008, 32, 1311−1313.

13. Climent, M. J.; Corma, A.; Iborra, S. Heterogeneous Catalysts for the One-Pot Synthesis of Chemicals and Fine Chemicals. Chem.Rev. 2011, 111, 1072−1133.

14. Shylesh, S.; Wagener, A.; Seifert, A.; Ernst, S.; Thiel, W. R. Mesoporous Organosilicas with Acidic Frameworks and Basic Sites in the Pores: An Approach to Cooperative Catalytic Reactions. Angew. Chem., Int. Ed. 2010, 49, 184−187.

15. Shiju, N. R.; Alberts, A. H.; Khalid, S.; Brown, D. R.; Rothenberg, G. Mesoporous Silica with Site-Isolated Amine and Phosphotungstic Acid Groups: A Solid Catalyst with Tunable Antagonistic Functions for One-Pot Tandem Reactions. Angew. Chem., Int. Ed. 2011, 50, 9615−9619.

16. Takagaki, A.; Takahashi, M.; Nishimura, S.; Ebitani, K. One-Pot Synthesis of 2,5-Diformylfuran from Carbohydrate Derivatives by Sulfonated Resin and Hydrotalcite-Supported Ruthenium Catalysts. ACS Catal. 2011, 1, 1562−1565.

17. Yang, Y.; Liu, X.; Li, X.; Zhao, J.; Bai, S.; Liu, J.; Yang, Q. A Yolk−Shell Nanoreactor with a Basic Core and an Acidic Shell for Cascade Reactions. Angew. Chem., Int. Ed. 2012, 51, 9164−9168.

18. Gianotti, E.; Diaz, U.; Velty, A.; Corma, A. Designing Bifunctional Acid-Base Mesoporous Hybrid Catalysts for Cascade Reactions. Catal. Sci. Technol. 2013, 3, 2677−2688.

19. Ganai, A. K.; Shinde, P.; Dhar, B. B.; Sen Gupta, S.; Prasad, B. L.V. Development of a Multifunctional Catalyst for a ″ Relay″ Reaction.RSC Adv. 2013, 3, 2186−2191.

20. Filice, M.; Marciello, M.; Morales, M. d. P.; Palomo, J. M. Synthesis of Heterogeneous Enzyme-Metal Nanoparticle Biohybrids in Aqueous Media and Their Applications in C-C Bond Formation and Tandem Catalysis. Chem. Commun. 2013, 49, 6876−6878.

21. Nelson, N. C.; Chaudhary, U.; Kandel, K.; Slowing, I. Heterogeneous Multicatalytic System for Single-Pot Oxidation and C−C Coupling Reaction Sequences. Top. Catal. 2014, 57, 1000−1006.

22. Kung, H.; Kung, M. Inspiration from Nature for Heterogeneous Catalysis. Catal. Lett. 2014, 144, 1643−1652.

23. Climent, M. J.; Corma, A.; Iborra, S.; Sabater, M. J.Heterogeneous Catalysis for Tandem Reactions. ACS Catal. 2014, 4, 870−891.

24. Li, H.; Fang, Z.; Smith, R. L.; Yang, S. Efficient Valorization of Biomass to Biofuels with Bifunctional Solid Catalytic Materials. Prog. Energy Combust. Sci. 2016, 55, 98−194.

25. Parlett, C. M. A.; Isaacs, M. A.; Beaumont, S. K.; Bingham, L.M.; Hondow, N. S.; Wilson, K.; Lee, A. F. Spatially Orthogonal Chemical Functionalization Of a Hierarchical Pore Network for Catalytic Cascade reactions. Nat. Mater. 2016, 15, 178−182.

26. Gaona, A.; Díaz, U.; Corma, A. Functional Acid and Base Hybrid Catalysts Organized by Associated (Organo)Aluminosilicate Layers for C−C Bond Forming Reactions and Tandem Processes. Chem. Mater. 2017, 29, 1599−1612.

27. Margelefsky, E. L.; Zeidan, R. K.; Davis, M. E. Cooperative Catalysis by Silica-Supported Organic Functional Groups. Chem. Soc. Rev. 2008, 37, 1118−1126.

28. Huang, Y.; Xu, S.; Lin, V. S. Y. Bifunctionalized Mesoporous Materials with Site-Separated Brønsted Acids and Bases: Catalyst for a Two-Step Reaction Sequence. Angew. Chem., Int. Ed. 2011, 50, 661−664.

29. Hong, J.; Lee, I.; Zaera, F. Correlated Bifunctionality in Heterogeneous Catalysts: Selective Tethering of Cinchonidine Next to Supported Pt Nanoparticles. Catal. Sci. Technol. 2015, 5, 680−689.

30. Park, M.; Kim, J. H.; Shim, I.-K.; Choy, J.-H. Fabrication of Pore Window in Ordered Mesoporous Silica by Spatial Control of Functional Groups. Chem. Eng. J. 2014, 253, 1−7.

31. Galloway, J. M.; Kung, M.; Kung, H. H. Synthesis and Characterization of Bifunctional Surfaces with Tunable Functional Group Pairs. Surf. Sci. 2016, 648, 284−290.

32. Mehdi, A.; Reye, C.; Brandes, S.; Guilard, R.; Corriu, R. J. P. Synthesis of Large-Pore Ordered Mesoporous Silicas Containing Aminopropyl Groups. New J. Chem. 2005, 29, 965−968.

33. Hong, J.; Lee, I.; Zaera, F. Cinchona Alkaloids Tethered on Porous Silica as Enantioselective Heterogeneous Catalysts. Top. Catal. 2011, 54, 1340−1347.

34. Hong, J.; Zaera, F. Interference of the Surface of the Solid on the Performance of Tethered Molecular Catalysts. J. Am. Chem. Soc. 2012, 134, 13056−13065.

35. Hong, J.; Djernes, K. E.; Lee, I.; Hooley, R. J.; Zaera, F. Heterogeneous Catalyst for the Selective Oxidation of Unactivated Hydrocarbons Based on a Tethered

Metal-Coordinated Cavitand. ACS Catal. 2013, 3, 2154−2157.

36. Alauzun, J.; Mehdi, A.; Reyé, C.; Corriu, R. J. P. Mesoporous Materials with an Acidic Framework and Basic Pores. A Successful Cohabitation. J. Am. Chem. Soc. 2006, 128, 8718−8719.

37. Zhao, D.; Feng, J.; Huo, Q.; Melosh, N.; Fredrickson, G. H.; Chmelka, B. F.; Stucky, G. D. Triblock Copolymer Syntheses of Mesoporous Silica with Periodic 50 to 300 Angstrom Pores. Science 1998, 279, 548−552.

38. Vinu, A.; Hossain, K. Z.; Ariga, K. Recent Advances in Functionalization of Mesoporous Silica. J. Nanosci. Nanotechnol. 2005, 5, 347−371.

39. Corma, A.; Garcia, H. Silica-Bound Homogenous Catalysts as Recoverable and Reusable Catalysts in Organic Synthesis. Adv. Synth. Catal. 2006, 348, 1391−1412.

40. Zaera, F. Nanostructured Materials for Applications in Heterogeneous Catalysis. Chem. Soc. Rev. 2013, 42, 2746−2762.

41. Pujari, S. P.; Scheres, L.; Marcelis, A. T. M.; Zuilhof, H. Covalent Surface Modification of Oxide Surfaces. Angew. Chem., Int. Ed. 2014, 53, 6322−6356.

42. Vig, J. R. UV/Ozone Cleaning of Surfaces. J. Vac. Sci. Technol., A 1985, 3, 1027−1034.

43. Guo, L.; Zaera, F. Spatial Resolution in Thin Film Deposition on Silicon Surfaces by Combining Silylation and UV/Ozonolysis. Nanotechnology 2014, 25, 504006.

44. Caravajal, G. S.; Leyden, D. E.; Quinting, G. R.; Maciel, G. E. Structural Characterization of (3-Aminopropyl)Triethoxysilane-Modified Silicas by Silicon-29 and Carbon-13 Nuclear Magnetic Resonance. Anal. Chem. 1988, 60, 1776−1786.

45. Albert, K.; Bayer, E. Characterization of Bonded Phases by Solid-State NMR Spectroscopy. J. Chromatogr. A 1991, 544, 345−370.

46. Krupczyńska, K.; Buszewski, B.; Jandera, P. Peer Reviewed: Characterizing HPLC Stationary Phases. Anal. Chem. 2004, 76, 226A−234A.

47. Ide, M.; El-Roz, M.; De Canck, E.; Vicente, A.; Planckaert, T.; Bogaerts, T.; Van Driessche, I.; Lynen, F.; Van Speybroeck, V.; Thybault-Starzyk, F.; et al. Quantification of Silanol Sites for the Most Common Mesoporous Ordered Silicas and Organosilicas: Total Versus Accessible Silanols. Phys. Chem. Chem. Phys. 2013, 15, 642−650.

48. Jones, C. W.; Tsuji, K.; Davis, M. E. Organic-Functionalized Molecular Sieves as Shape-Selective Catalysts. Nature 1998, 393, 52−54.

49. Müller, M.; Harvey, G.; Prins, R. Comparison of the Dealumination of Zeolites Beta, Mordenite, ZSM-5 and Ferrierite by Thermal Treatment, Leaching with Oxalic Acid and Treatment with SiCl4 by 1H, 29Si and 27Al MAS NMR. Microporous Mesoporous Mater. 2000, 34, 135−147.

50. Lippens, B. C.; de Boer, J. H. Studies on Pore Systems in Catalysts. J. Catal. 1965, 4, 319−323.

51. Scherdel, C.; Reichenauer, G.; Wiener, M. Relationship between Pore Volumes and Surface Areas Derived from the Evaluation of N2-Sorption Data by Dr-, Bet- and T-Plot. Microporous Mesoporous Mater. 2010, 132, 572−575.

52. Palomo, C.; Oiarbide, M.; Laso, A. Recent Advances in the Catalytic Asymmetric Nitroaldol (Henry) Reaction. Eur. J. Org. Chem. 2007, 2007, 2561−2574.

53. Guan, J.; Liu, B.; Yang, X.; Hu, J.; Wang, C.; Kan, Q. Immobilization of Proline onto Al-SBA-15 for C−C Bond-FormingReactions. ACS Sustainable Chem. Eng. 2014, 2, 925−933.

54. Biradar, A. V.; Patil, V. S.; Chandra, P.; Doke, D. S.; Asefa, T. A Trifunctional Mesoporous Silica-Based, Highly Active Catalyst for One-Pot, Three-Step Cascade Reactions. Chem. Commun. 2015, 51,8496−8499.

55. Lauwaert, J.; Moschetta, E. G.; Van Der Voort, P.; Thybaut, J.W.; Jones, C. W.; Marin, G. B. Spatial Arrangement and Acid Strength Effects on Acid−Base Cooperatively Catalyzed Aldol Condensation on Aminosilica Materials. J. Catal. 2015, 325, 19−25.

Chapter 3: Construction of 2nd-Generation Acid-Base Heterogeneous Tandem Catalysts with Cinchonidine and Phosphonic Acid

In this chapter, a new dual acid−base system was constructed by combining our protocol in Chapter 2 and "click" chemistry. Mesoporous SBA-15 was functionalized with Cinchonidine, which introduces chiral sites, and phosphonic acid was first time prepared via the following steps:

(1)addition of Ethoxy-protected phosphonic-linked triethoxysilanes ((2-diethylphosphatoethyl) triethoxysilane);

(2)controlled use of UV/ozonolysis to selectively remove the exterior groups;

(3)decoration of the exterior sites freed in Step 2 with cinchonidinyl (3-triethoxysilylpropyl) carbamate;

(4)Ethoxy deprotection of the 2-diethylphosphatoethyl groups to phosphonic acid by acidolysis;

This newly synthesized material is functionalized with cinchonidine groups on the external surfaces and entrance of the pores and phosphonic acid inside those tunnels, at coverage ratios that can also be tuned by controlling the UV/ozonolysis length. The samples were fully characterized by ^{31}P, ^{29}Si and ^{13}C solid-state NMR, acid−base titrations, CNS elemental analysis, and N_2 adsorption isotherms measurements. And the recovery process of silanols via UV/O_3 treatment was investigated. Those catalysts were successfully tested for the promotion of a couple of reactions including Deacetalization-Henry cascade reaction, Cyano-Ethoxycarbonylation reaction and 1,4-addition of thiols to cylic

enones (Sulfa-Michael addition). The promoting effect for silanol groups was further studied for Deacetalization-Henry cascade reaction.

3.1 Introduction

One added advantage of creating acidic and basic sites on solids via the tethering of molecular functionalities is that those all display uniform chemistry and the same acid/base strength (in contrast, most acidic solids display a distribution of sites with different acid strengths). However, although the initial 1st-Generation **HSO_3-(NH_2- SBA-15)** catalyst exhibits fully functional for simple Deacetalization-Henry reaction, it only provides its acidic and basic functionality; more challenging processes may require tunability, more functionalities, and a greater range of acidity/basicity in the sequestered groups.

In the 1st-Generation catalyst, synthetic variation of the acid and base groups is highly limited due to the H_2O_2 oxidation step that converts the thiol group to a sulfonic acid: the primary amine group must be protected, in our case by Boc- groups, to prevent oxidative degradation, limiting the scope of groups that can be attached. **Figure 3.1(b)** shows a range of systems that would allow systematic variation of basicity in the attached functional groups. The primary amine (NH_2-) currently employed has a pKa of 10.59, but the number of reactions accessible using such base is limited by the innate nucleophilicity of that group. A far wider scope of reactivity may be possible via the introduction of pyridyl (pKa = 6.5), imidazole (pKa = 7.75), or the quinuclidine unit from quinine (QN, pKa = 7.73). Incorporation of these motifs to our pool of molecular catalytic units to be tethered to the mesoporous scaffold will confer four orders of magnitude variation in basicity on the resulting system. Each of these groups can be introduced to the oxide support by synthesizing the corresponding triethoxysilane derivative, made via Pt-mediated hydrosilylation of the commercially available olefin precursors.[1]

In this thesis, a cinchona alkaloid, cinchonidine, will be introduced to SBA-15 surface as new basic groups. Cinchona alkaloids were initially obtained from extracting the bark of Cinchona species. The curative properties were known even earlier than its chemical properties: local residences usually took the powder of cinchona ledgeriana bark to prevent malaria in the late 1500s. But its scientific identification was made much later. The major species, quinine and cinchonine, were successfully extracted by P.Pelletier in 1820 and other key alkaloids were later identified. Those cinchona alkaloids have been proven quite useful in many fields. Medically, they were used to treat malaria[2,3] and cardiac arrhythmias[4]. In common life, they have been used as food additives[5] for their special flavor, like the bitter flavor in tonic water. Besides, for their chemical applications, cinchona alkaloids have been used as chiral resolving agents in chromatography [6,7] and also found particular use in catalysis, for both homogeneous reactions [8-10] and, as modifiers, in heterogeneous systems.[11,12]

However, although cinchonidine has been quite commonly used as a homogeneous catalyst, it is still worth of heterogenizing this cinchona alkaloid by tethering it onto a solid support, which will solve the most typical limitation for homogeneous catalyst: separate and recycle. Scientists have reported several “heterogenizing” works with organometallic catalysts,[13,14] and have extended those application to enhance the catalytic activity of typical supports such as alumina or silica.[15-17]

Our group has previously reported a successful construction work of anchoring cinchonidine onto a high surface-area silica.[18,19] With this new “click” chemistry, we will be able to introduce cinchonidine into our bifunctional system. The introduction of cinchona

alkaloid derivatives to the surface offers two advantages: the quinuclidine group is very strongly basic, and the group is homochiral, introducing the possibility of chiral induction and asymmetric catalysis.

Besides, neither cinchonidine nor none of the basic groups shown in **Figure 3.1(b)** are compatible with the thiol-to-sulfonic acid oxidation step previously used to add the acidic groups to the oxide for 1st-generation catalyst, so a different attachment procedure and species for the acid will be required to make the 2nd-generation acid-base catalysts as well. Some options here include carboxylic-acid and phosphonic-acid. The first one can be obtained by carboxylic-acid tert-butyl ester-linked triethoxysilanes, which can be easily converted to carboxylic-acid species via pyrolysis.[20] And our choice, phosphonic acid can be obtained via an ethoxy protected phosphonic-acid-linked triethoxysilanes,[21] which are commercially available.

In this chapter, we will continue using our developed methodology to Construct 2nd-Generation acid-base heterogeneous tandem catalysts with Cinchonidine and phosphonic acid. The resulting catalysts were thoroughly characterized to corroborate the success of the synthetic approach.

The details of this work follow.

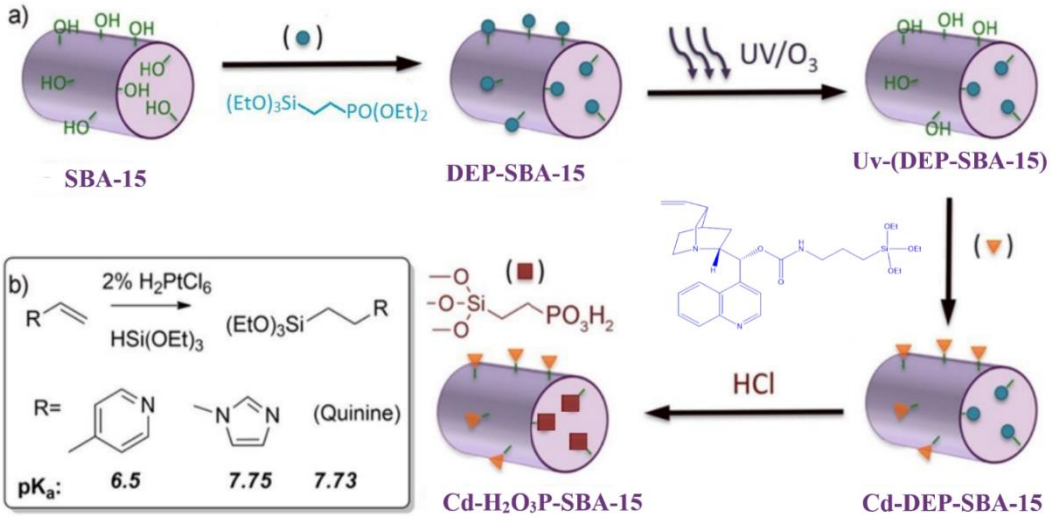

Figure 3.1 Synthetic strategy used in this research for the preparation of 2nd-Generation acid−base catalyst catalysts.

3.2 Experimental Details

Most of the chemicals used, including the SBA-15, were purchased from Sigma-Aldrich (research purity) and used as supplied.

A new approach was applied in grafting both acidic (phosphonic acid) and basic (cinchonidine) moieties to an SBA-15 mesoporous support[18,19,22] according to methodology in Chapter 2, as shown in **Figure 3.1**. The synthetic steps were the following:

1. Tethering of DEP- to the surfaces of SBA-15 (Step 1, to make **DEP-SBA-15**):

SBA-15 (1 g) was calcined under vacuum at 200 °C for 2 h, then was dispersed in 20 mL of anhydrous toluene. After that, 1.5 ml of (2-diethylphosphatoethyl) triethoxysilane (**DEP**) was introduced into the flask under a nitrogen atmosphere at room temperature. The condensation was conducted at 110 °C for 24 h, and it was followed by filtering, washing with toluene, and drying under vacuum overnight.

2. Selective removal of DEP- groups from the outside and pore-entrance surfaces (Step 2, to make **UV-(DEP-SBA-15)-3h**):

The **DEP-SBA-15** samples were exposed to a combination of ultraviolet (UV) radiation and ozone for various hours (i.e. 3 hours), using a Spectrolinker XL-1500 UV cross-linker instrument equipped with both its original λ (wavelength) = 254 nm lamp and an additional λ = 185 nm radiation source (to produce ozone from molecular oxygen).[23,24] The UV power was set to 10 000 μW/cm^2. The resulting samples were named as **UV-(DEP-SBA-15)-xh**, where x indicates the ozonolysis time.

3. Tethering of Cd- groups to the outside and pore entrance surfaces (Step 3, to make **Cd-Uv(DEP-SBA15)-3h**):

The Cd−TEOSPC (0.0042 mol) was dissolved in ethanol (20 mL) and added to the Uv-DEP-SBA15 (0.5 g), and that mixture was refluxed at 83 °C for 48 hours. The final product, **Cd-Uv(DEP-SBA15)-3h**, was let to cool down, filtered, then washed with ethanol (150 mL), toluene and/or diethyl ether (50 mL), and dried in vacuum before use.

4. Deprotection of DEP groups in **Cd-Uv(DEP-SBA15)-3h** to $-H_2PO_3$ (Step 4, to make **Cd-Uv-H_2O_3P-SBA15-3h**):

0.5 g of **Cd-Uv(DEP-SBA15)-3h** was stirred in 10 mL of saturated HCl at room temperature under N_2 atmosphere for 24 h. The solid was filtered and washed with deionized water until the pH value of the filtrate reached a value close to 7, and dried overnight under vacuum.

Synthesis of cinchonidinyl(3-triethoxysilylpropyl)carbamate (**Cd-TEOSPC**):

The carbamate-linked catalysts were made by first dissolving the cinchonidine (0.015 mol) in THF (70 mL), adding the ICPTEOS (0.018 mol) together with a small amount of dibutyltindilaurate (0.0015 mol). Then refluxing at 70 ^{o}C for 3h. Let the solution cooled down and rested for a day. Then the solvent(THF) was evaporated and pentane (100 mL) was added to precipitate the new compound (cinchonidinyl(3-triethoxysilylpropyl) carbamate) (Cd− TEOSPC). After filtering and washed with more pentane. The resulting material was dried under nitrogen.

The ^{31}P, ^{29}Si and ^{13}C cross-polarization magic-angle spinning (CP/MAS) NMR data were acquired on a Bruker Avance 600 spectrometer equipped with a 4 mm H/X CP-MAS probe operating at 119.2 MHz. All spectra were recorded employing a spinning speed of 10 kHz. For the ^{29}Si CP/ MAS NMR spectra, a cross-polarization contact time of 2 ms, a

^{1}H decoupling bandwidth of 80 kHz, and a recycle time of 3s were used. Data were acquired as 12000 coadded 2048 complex data point FIDs with a 100 kHz sweep width. Post-acquisition processing consisted of exponential multiplication with 200 Hz of line broadening and zero filling to 4096 data points. Chemical shifts were referenced to an external DSS sample.

The surface concentrations of the phosphonic acid and cinchonidine groups were quantified by acid−base back-titrations and CNS flash elemental analysis(EA). The cinchonidine coverages were estimated by neutralizing the catalysts (25 mg) with HCl solution (5 mL, 0.0224 M), filtering the solid and quantitative collecting the solution, and titrating the filtrate with a NaOH solution (0.01 M), using phenolphthalein as the indicator. The acidic groups were estimated by first reacting the solid with a known excess of Na_2CO_3 (4 mL, 0.01M solution) and treating the filtered solution with a fixed excess of HCl (5 mL, 0.0244 M solution) before titrating with NaOH (0.01 M), again using phenolphthalein as the indicator. The cinchonidine contents were also analyzed with flash EA. CNS elemental analysis was carried out by Flash EA1112 instrument. Cinchonidine contents from acid-base titration and EA were quite similar.

The surface areas, pore volumes, and pore size distributions were estimated from N_2 adsorption−desorption isotherms obtained using a commercial 2000e Model 25 Nova Win vacuum volumetric gas sorption system. The data were analyzed by using the Barrett−Joyner−Halenda (BJH) isotherm equations on desorption branches of the data.

The Deacetalization-Henry cascade reactions were carried out as follows: the catalyst (50 mg or as indicated in the table) was first heated at 50 °C for 2 h under vacuum to remove

any absorbed water. Nitromethane (4 mL) and benzaldehyde dimethyl acetal (0.5 mmol) were added under a nitrogen atmosphere, and the mixture was stirred at 90 °C, still under nitrogen. Aliquots (0.1 mL) were taken at different time intervals to monitor the reaction progress; they were analyzed by gas chromatography, using a HP-50 column, to determine the yields of benzaldehyde and β-nitrostyrene (2-nitrovinylbenzene).

Cyano-Ethoxycarbonylation reactions were carried out as follows: toluene (2.5ml), ethyl cyanoformate (0.5mmol), and benzaldehyde (0.25 mmol) were mixed in a vial. 8 mol% amount(based on benzaldehyde) of catalyst was added into resulting solution(0.020mmol cinchonidine). The mixture was vigorously stirred at room temperature under a nitrogen atmosphere for 30h. 0.1 mL solution were taken after reaction and analyzed by GC-MS. ee% values are obtained from gas chromatography equipped with chiral column.

1,4-addition of thiols to cylic enones reactions were carried out as follows: benzene (3ml), p-tertbutylbenzenethiol (1.81mmol), and 2-cyclohexene-1-one (1.56 mmol) were mixed in a vial. Then 1 mol% amount(based on ketone) of catalyst was added (0.015mmol cinchonidine) in resulting solution. The mixture was vigorously stirred at room temperature under a nitrogen atmosphere for 24h. 0.1 mL solution were taken after reaction and analyzed by GC. The crude product was obtained by flash column chromatography on silica gel and its optical activity was measured in a chloroform solution using a MC 241 polarimeter with a Na lamp (λ = 589 nm).

3.3 Catalyst Characterization: ^{13}C and ^{31}P CP/MAS NMR

The integrity of the tethered organic moieties was checked with ^{13}C CP/MAS NMR first. The data from a typical ^{13}C CP/MAS NMR characterization sequence is shown in **Figure 3.2**. The peak assignments are summarized in **Table 3.1**.[22,25] The ^{13}C NMR spectra data for cinchonidine and phosphonic precursor are shown in Supporting data at the end of this chapter. As illustrated, for the case of the **DEP-SBA-15** (second from the top) intermediate (Step 1), all the peaks match the peak assignment for DEP- groups well. Besides, similar **DEP-SBA-15** ^{13}C CP/MAS NMR peaks are observed in the trace after 3 hours UV/O3(third from the top) except for the peak at 15.7 and 16.8 ppm combined to a "shoulder peak" shape, which may cause by the easier accessibility for ozonolysis of the outer part(C4 and C6. The addition of cinchonidine moieties (Step 3, fourth trace from top) leads to a quite changed spectrum due to the large peak range of cinchonidine. Despite those overlaps, the unique peak for DEP- at 4.2ppm still remains in all the materials, which can be treated as an evidence of the appearance of phosphonic moieties. Also, after grafting cinchonidine, the treated material shows a quite same pattern with **Cd-SBA15**(top trace), in which SBA-15 was functionalized with only cinchonidine, and with Cd- precursor (data not shown). Especially, the peaks from 140 to 150 ppm assigned to quinoline rings in **Cd-Uv(DEP-SBA15)-3h** well confirmed the successfully tethering of cinchonidine onto SBA-15. The spectrum for the final **Cd-Uv-H_2O_3P-SBA15-3h**) sample can be well-assigned with all cinchonidine peaks in the table which indicates well-preserved cinchonidine function at phosphonic deprotect after Step 4 (bottom trace). However, it does show some significant differences including the following: (1) the

increase of peaks at 9.9 ppm, which is actually due to the decreases for peaks 16.8 ppm(C6 for DEP-) since during the deprotection process, the ethoxy part will be detached from surface. (2) the conjunction of two peaks at ~26 ppm (C4, C5 for quinuclidine ring) and increase and slightly shift of peak at 157 ppm may be associated with remaining absorption water during the deprotection process. More studies need to be done in the future to figure it out.

Despite well-defined peaks for cinchonidine moieties in ^{13}C CP/MAS NMR, these spectra did not give us solid evidence for the status for DEP- grafting work. Thus, ^{31}P solid state NMR which is specially designed for those phosphorous containing chemicals were performed for all resulting material from Step 1 to Step 4. Those results are shown in **Figure 3.3**. All traces in this figure represents a same peak pattern with a major peak at 34.3 ppm and a couple of minor peaks symmetrically distributed from major peak. Those minor peaks may come from insufficient spinning during ^{31}P NMR measurement.[22] The major peak at 34.3 ppm is attributed to both DEP- and deprotected phosphonic acid since they share a quite same chemical shift in ^{31}P CP/MAS NMR spectra.[22,26] This unchanged peak position not only indicates a successfully DEP- grafting work in Step 1, but also suggests those phosphonic moieties are preserved well upon following Uv/O_3 treatment (Step 2), cinchonidine tethering (Step 3), and deprotection.

^{13}C and ^{31}P CP/MAS NMR spectra here indicate that a dual cinchonidine-phosphonic acid bifunctional catalyst has successfully been prepared via our synthetic strategy shown in **Figure 3.1.**

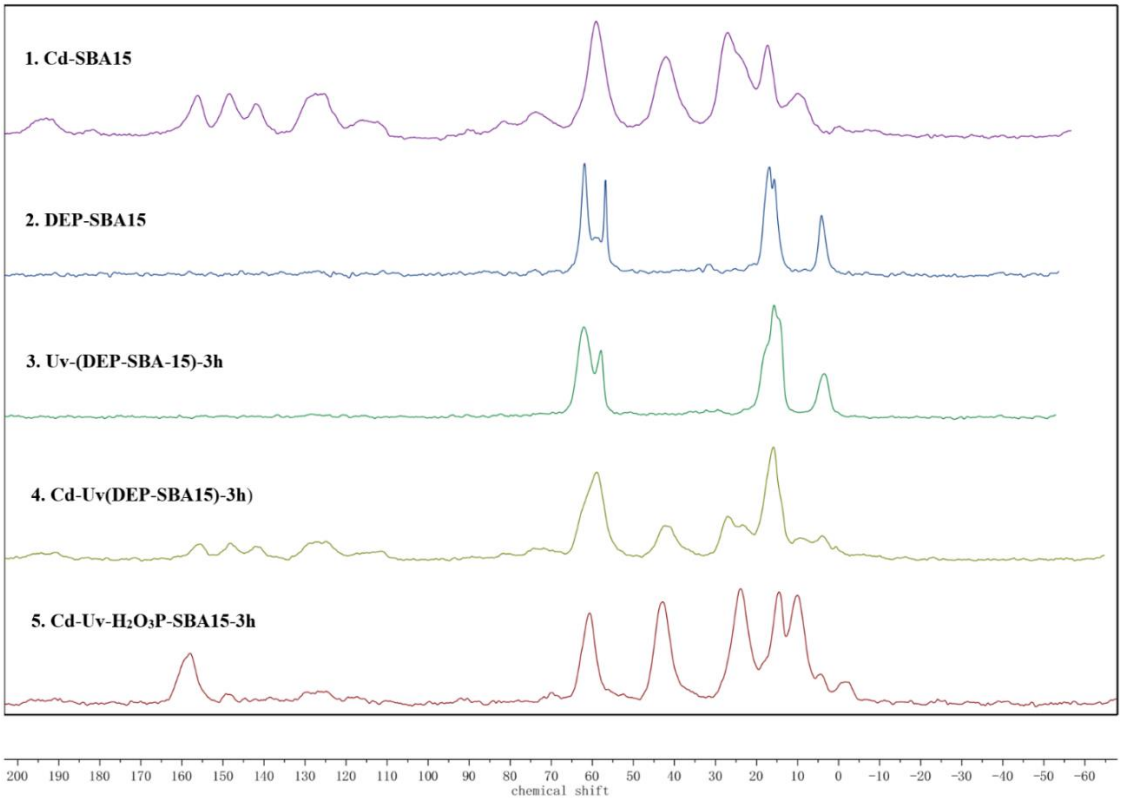

Figure 3.2 ^{13}C CP/MAS NMR spectra from our SBA-15-based catalysts after each synthetic step, as indicated in Figure 3.1. The peak assignment is provided in **Table 3.1**.

Table 3.1 Peak assignment for ^{13}C CP/MAS NMR spectra in **Figure 3.2**. Figure below demonstrates peak assignments for DEP- part.

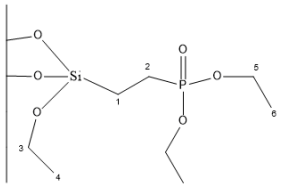

Shift d/ppm	Assignment
	Cd peaks: 1. Quinuclidine and alcohol carbon
22.1	C7
26.7	C5
26.9	C4
39.7	C3 (carbon next to vinyl)
43.5	C6
56.6	C2
59.9	C8 (Corner C next to COH)
74.0	C9 (carbon in C–O)
	Cd Peaks: 2. Quinoline ring and vinyl
114.5	C11 (vinyl, CH2 carbon)
118.9	C5' (benzene ring)
123.6	C3' (pyridine ring)
125.4	C9' (benzene-pyridine bridge)
126.7	C6' (benzene ring)
129.1	C7' (benzene ring)
130.6	C8' (benzene ring)
141.8	C10 (vinyl, CH carbon)
148.8	C10' (benzene-pyridine bridge)
150.1	C2' & C4' (pyridine ring)
	ICPTEOS peaks
9.9	First carbon bond in propyl moiety, carbon in C–Si
17.5	Methyl carbon in ethoxy moiety
23.4	Second carbon in propyl moiety
42.2	Third carbon in propyl moiety, next to carbamate
58.9	Methylene carbon in ethoxy moiety Carbamate peaks
156.6	C=O in link Cd-TEOSPC (–O–CO–NH–)
	DEP- and H_2O_3P- peaks
4.2	C1, carbon connected with silica
15.7	C2, ethyl carbon next to P
15.7	C4, terminate carbon in ethyl group
16.8	C6, terminate carbon in protection DEP group
57.9	C3, first carbon in Si-O-ethyl part
62.1	C5, carbon next to phosphonic acid

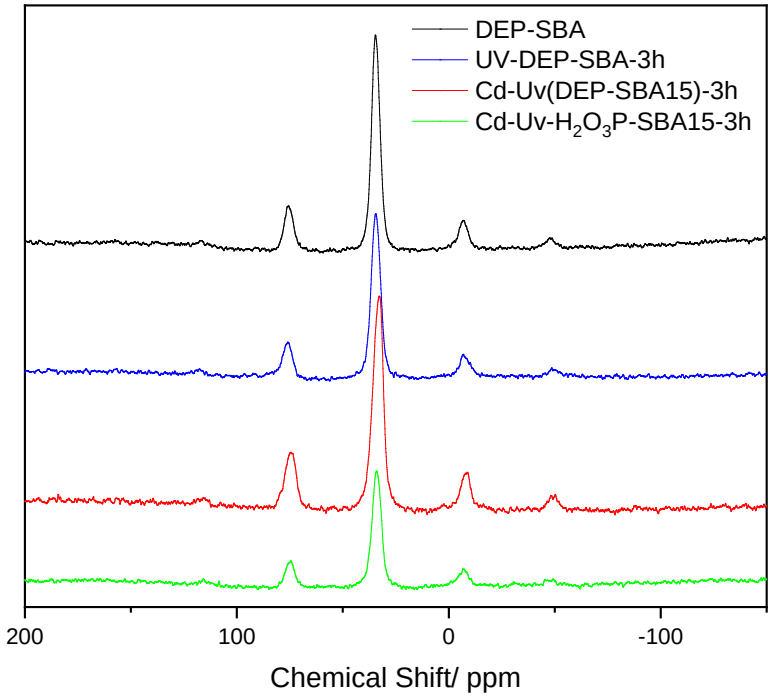

Figure 3.3 ^{31}**P** Solid-state NMR data for different stages of functionalized SBA15. All minor peaks are from insufficient spinning

3.4 Catalyst Characterization: N_2 Adsorption Isotherms and function moiety content

Texture properties of catalysts were carried out by N_2 adsorption isotherms. Due to the well-defined, stable tunnel structure of SBA-15, that our samples all show Barrett-Joyner-Halenda (BJH) type IV isotherm behavior (data not shown), as is characteristic of well-maintained ordered mesoporous materials.[27,28] Additional data can be extracted in terms of total surface area and pore volume as well. Pore size distributions(from desorption branch) obtained from our studies are displayed in **Figure 3.4** and **Figure 3.5.** And all results are summarized in **Table 3.2**.

Figure 3.4 indicates results for DEP-SBA15 treated with different UV/O_3 treatment length (Step 2) and the exact value shown in entry 1 to entry 5 in **Table 3.2.** There are significant losses of surface area and total pore volume upon the initial grafting of Ethoxy-protected phosphonic groups (Step 1), and the average pore diameter is reduced by approximately 0.9 nm. By employing Uv/ozonolysis treatment, samples treated with 3 hours and 5 hours represent a bimodal distribution for pore size, which may indicate a slow removal process for the outer part and a well-maintain inner pore. **DEP-SBA-15** treated with only 10 minutes Uv/O_3 doesn't appear that a distribution shape, due to a too short ozonolysis time. Anyway, all samples appear a slight increase in surface area and pore volume, upon UV/O_3 treatment. And by prolonging Uv/O_3 time, those values will further increase, which suggests we are able to remove surface DEP- groups via UV/O_3 treatment slowly.

Figure 3.5 and Entry 1,2,4,6,7 illustrates the overall construction procedures. After significant losses and slight increases of surface area and pore volume as we discussed

above. They dramatically decrease again in Step 3, upon the addition of large basic functionality cinchonidine groups. And finally, those values go up again as the Ethoxy-protecting groups are removed from the phosphonic moieties (Step 4). The changes are in general corresponding with our procedures.

A further study of grafting process was done by Multi-peak Gaussian fitting in **Figure 3.6** and fitting results are shown in **Table 3.3.** Three fitted pore sizes are worth pointing out here: 5.02nm, 5.41nm, 5.84nm, which can be assigned to cinchonidine grafted part, DEP- grafted part and Uv/ozonolyzed DEP- grafted part, respectively. As shown in Entry 2,4,5 in **Table 3.3**, by employing UV/O_3 treatment, the percentage of the peak at 5.41nm decrease along with an increase of peak at 5.84nm. This trend implies the successful removal process by Uv/ozonolysis process. However, the sample treated with 10min Uv/O_3 does comply with this trend. That may cause by the error introduced by this quite short treatment compared with other entries, which has only very few effects on the increase of pore size. Besides, a completely disappear of peak at 5.84, which represents Uv/ozonolyzed DEP- grafted part, along with the appearance of a new peak at 5.02nm also comply with the introduction of cinchonidine moieties in Step 3. It can further confirm our successful construction of acid-base bifunctional catalyst.

Some semiquantitative estimate can be assumed by combing Gaussian fitted pore size and moieties contents. Moieties contents for both acid and base were obtained from acid-base titration method. Besides, the base (cinchonidine) content was further calculated from CNS elemental analysis, which shows a similar result with titration.

From what we can observe in **Table 3.6**, acid content obtained by titration are quite linear with “acid” peak volumes. It might suggest semiquantitative estimate for acid content by Gaussian fitted pore size and volume. However, extra errors might be introduced during Gaussian fitting serval samples together and incompleted deprotection may often happen. This semiquantitative estimate should therefore be taken with a grain of salt.

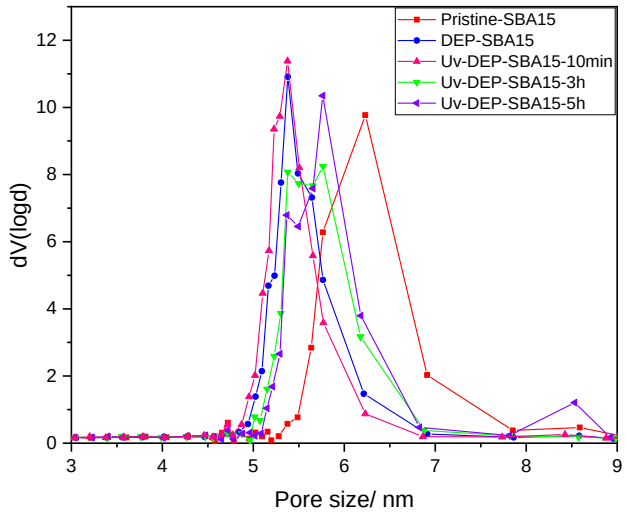

Figure 3.4 Pore size distribution for UV/O_3 treated DEP-SBA15, treatment length are 10min, 3h and 5h. Pore sizes are from desorption branch.

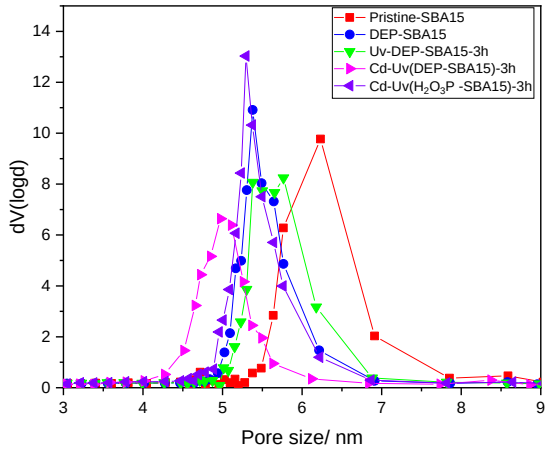

Figure 3.5 Pore size distribution for different stages of UV/O_3 functionalized SBA15. Pore sizes are from desorption branch.

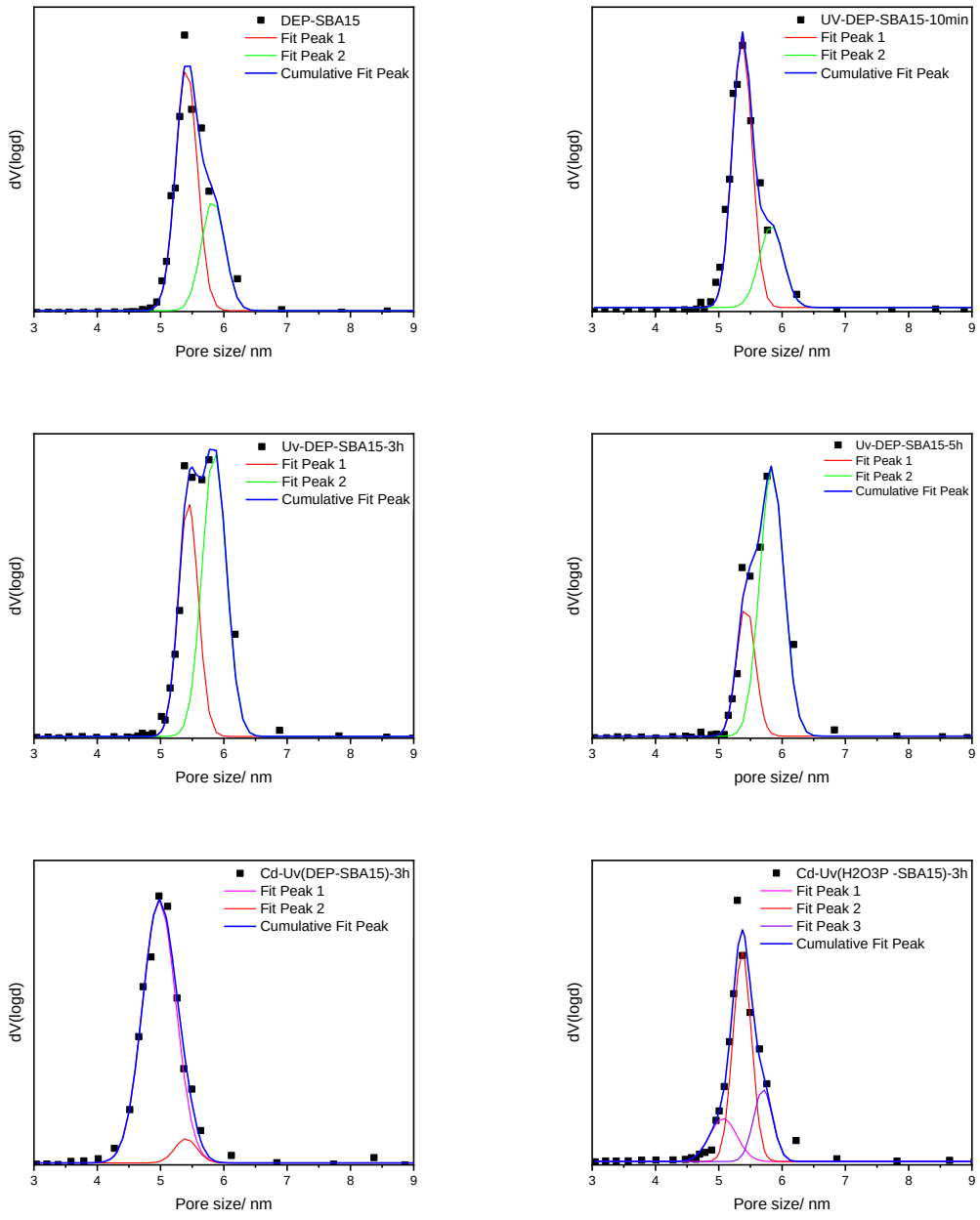

Figure 3.6 Multi-peak Gaussian fitting of functionalized SBA15.

Table 3.2 BET analysis for DEP-SBA15 and samples with different UV/O_3 treatment length
[a] V_T = total pore volume
[b] Calculated using the Barrett−Joyner−Halenda (BJH) equation on the desorption branch.
[c] Calculated pore sizes come from double peak Gaussian fitting. The average pore size for pore 1 is 5.41±0.04nm, pore 2 is 5.84±0.01nm and pore 3 is 5.02±0.04nm.
[d] Cd-Uv(H_2O_3P -SBA15)-3h fitted in tri-peak Gaussian fitting.

Entry	Sample	BET /m^2g^{-1}	V_t [a] /cc g^{-1}	Pore size [b] /nm	Calculated Pore size [c] /nm
1	Pristine-SBA15	677.70	0.914	6.23	N/A
2	DEP-SBA15	438.23	0.635	5.39	5.41&5.83
3	Uv-DEP-SBA15-10min	462.16	0.653	5.39	5.37&5.83
4	Uv-DEP-SBA15-3h	488.82	0.658	5.39 & 5.74	5.44&5.85
5	Uv-DEP-SBA15-5h	489.81	0.664	5.39& 5.74	5.43&5.84
6	Cd-Uv(DEP-SBA15)-3h	361.80	0.564	5.04	4.98&5.40
7	Cd-Uv(H_2O_3P -SBA15)-3h [d]	505.72	0.716	5.29	5.07&5.37&5.70

Table 3.3 Gaussian fitted results for DEP-SBA15 and samples at different stages.
[a] V_T = total pore volume
[b] Volume of peak 1=$\frac{Area\ of\ peak\ 1}{Area\ of\ peak\ 1 + Area\ of\ peak\ 2}$*total pore volume

Entry	Sample	V_t [a] /cc g^{-1}	Relative area ratio of peak 1[b]	Relative area ratio of peak 2[b]	Volume of peak at 5.41nm /cc g^{-1}	Volume of peak at 5.84nm /cc g^{-1}	Volume of peak at 5.02nm /cc g^{-1}
1	Pristine-SBA15	0.914	N/A	N/A	N/A	N/A	N/A
2	DEP-SBA15	0.635	0.67	0.33	0.426	0.210	N/A
3	Uv-DEP-SBA15-10min	0.653	0.73	0.27	0.476	0.176	N/A
4	Uv-DEP-SBA15-3h	0.658	0.40	0.60	0.263	0.395	N/A
5	Uv-DEP-SBA15-5h	0.664	0.27	0.73	0.179	0.485	N/A
6	Cd-Uv(DEP-SBA15)-3h	0.564	0.94	0.06	0.034	N/A	0.530
7	Cd-Uv(H_2O_3P -SBA15)-3h	0.716	N/A	N/A	N/A	N/A	N/A

Table 3.5. Moieties contents for functionalized SBA15
[a] Cinchonidine groups contents are calculated from CNS Flash EA analysis
[b] Acid group contents are calculated from acid titration method.

Sample	Cd- content/mmol*g-1[a]	Acid content/mmol*g-1[b]
Cd-SBA15	0.704	N/A
H_2PO_3-SBA15	N/A	0.608
Uv-(H_2PO_3-SBA15)-3h	N/A	0.352
Cd-Uv-H_2O_3P-SBA15-3h	0.229	0.166
Cd-Uv-H_2O_3P-SBA15-5h	0.441	0.067

Table 3.6 Titration data versus volume of peak at 5.41nm. Diagram below demonstrates a linear dot distribution.

Sample	Acid content/mmol*g-1	Volume of phosphonic peak/cc g^{-1}
H_2PO_3-SBA15	0.608	0.426
Uv-(H_2PO_3-SBA15)-3h	0.352	0.263
Cd-Uv-H_2O_3P-SBA15-3h	0.166	0.150

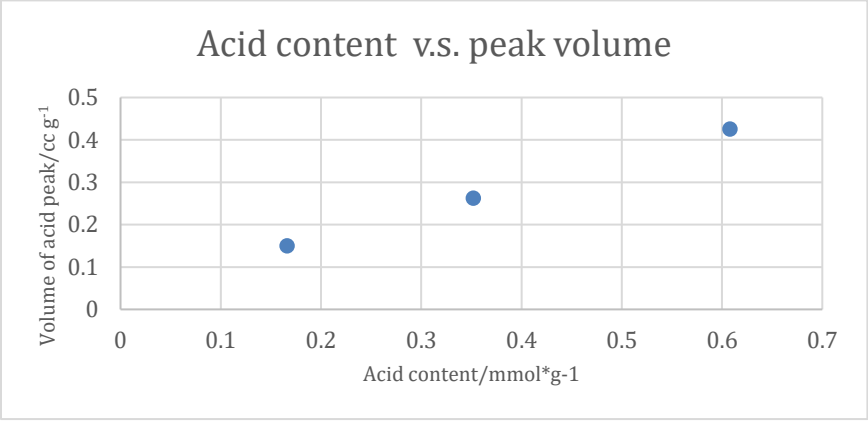

3.5 Catalyst Characterization: ^{29}Si CP/MAS NMR

The overall tethering and Uv/O_3 removal process was further evaluated via ^{29}Si CP/MAS NMR as supplement evidence. The results and T peak area percentage (a ratio to Q peaks, the signals from the nonderivatized Si−OH groups)are summarized in **Figure 3.7**. Upon DEP- grafting work in Step 1, the values for the T peak areas, which can be treated as the signal from the tethered species, dramatically increased to around 30%. Then **DEP-SBA-15** was treated with Uv/O_3 and causes a slight decrease in this area due to ozonolysis removal and silanols recovery. This total tethered groups content was increase again, in Step 3 by the addition of cinchonidine groups and finally decrease for a second time after deprotection. This decreases in derivatized Si may come from some detached functional moieties during deprotection and imply the existent of unlinked -Si-OC_2H_5 "tail" in DEP- silane precursor (C3&C4 of DEP- in **Table 3.1)**, which is inevitable during the grafting of DEP- groups.[21,22]

Further, the recovery of silanols via Uv/ozonolysis was studied by employing a much longer Uv/O_3 treatment time. The **DEP-SBA15** in this case was treated for 5 days(120 h). **Figure 3.8** represents this ^{29}Si solid state NMR spectra. As we observed in the bottom trace in **Figure 3.8**, almost no T peak (which represents derivatized Si-) can be observed in this **Uv-DEP-SBA15-120h** sample and the peak pattern is quite similar with unmodified SBA-15 shown in the top trace. Besides, by estimating percentage recovery of silanols,[29] 92% silanols have been recovered after 120-hour Uv/Ozonolysis, comparing with pristine SBA-15. This suggests that Uv/ozonolysis process is capable of removing grafted parts and recovering surface silanols. Besides, if we re-graft this **120h Uv/O_3**

treated DEP-SBA-15 with DEP- once more, the acid content will reach 0.625 mmol/g, which is slightly higher than 0.608 mmol/g for **DEP-SBA-15**. This insignificant increase may cause by extra Silicon sites introduced by the "click" chemistry. In Step 1, free -Si-OH groups are tethered with a functionalized silane, R'O-**Si'**-R(DEP- in our case), by forming a "Si-O-**Si'**-R" link. Uv/O_3 treatment can completely remove the -R parts in that link but it won't cut all of "Si-O-**Si'**" bond off. As a result, those new grafted **Si'** might introduce some fresh sites for re-derivation after a long-time removal process. That may slightly increase acid content.

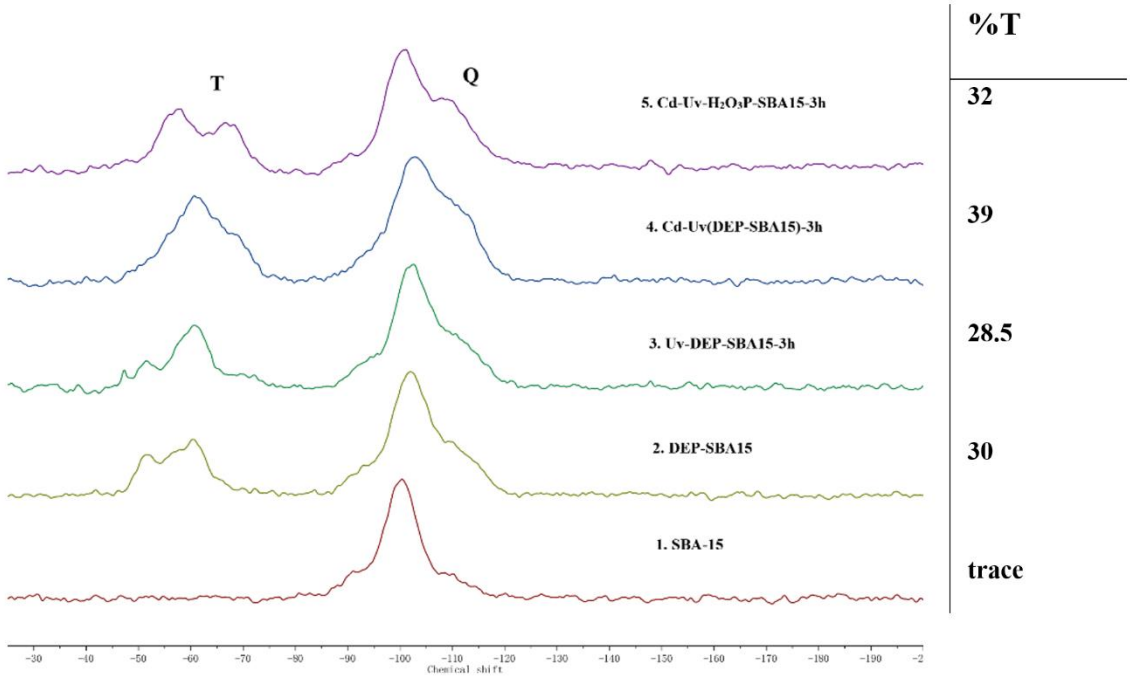

Figure 3.7 ^{29}Si cross-polarization magic-angle-spinning (CP/MAS) NMR spectra for pure SBA-15 and our SBA-15-based catalysts after each synthetic step, as indicated in **Figure 3.1**. T peak area percentages were shown at the right of the figure.

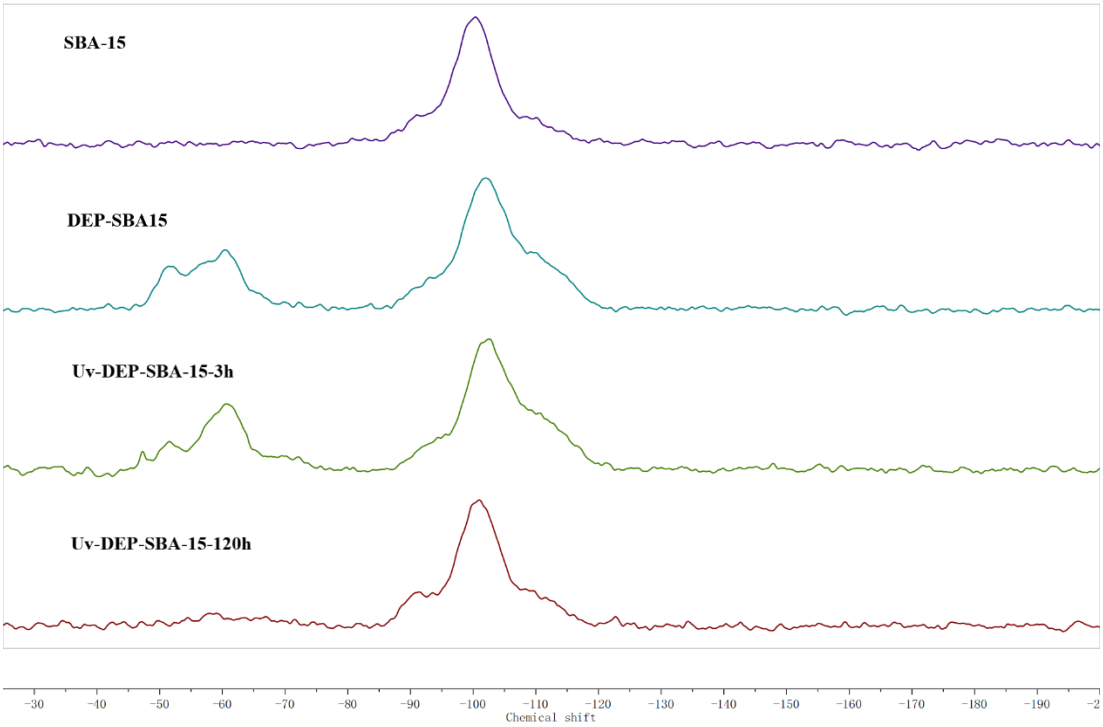

Figure 3.8 ^{29}Si cross-polarization magic-angle-spinning (CP/MAS) NMR spectra for DEP-SBA-15 treated with 120 hours Uv/O_3

3.6 Various Catalytic Performance

3.6.1 Deacetalization-Henry cascade reaction

2nd-Generation Dual Acid−Base Catalysts acid−base catalysts made by our synthetic procedure were first tested with Deacetalization-Henry cascade reaction which is usually treated as a probe for acid−base bifunctional catalysis.[30-32] Individual acid and base catalyzed steps were first examined. **Table 3.7** shows the results for the individual acid reaction. It suggested that neither a blank system nor plain **SBA1**5 can promote the reaction from dimethyl acetal to benzaldehyde. In entry 3, basic functionalities show no effect on this acid step either. Besides, no yield of β-nitrostyrene for all entries despite good conversions can be found in acid catalysts entries(Entry 4 and 5) may indicate phosphonic acid contained catalyst is quite efficient in promoting the first step, from dimethyl acetal to benzaldehyde, but cannot help with the promotion of nitromethane addition. **Table 3.8** shows base-catalyzed henry reaction. The first three entries in **Table 3.8** indicate that blank system, plain **SBA15** and phosphonic acid groups have no effect on this step. Cd-SBA-15 and our bifunctional catalyst in Entry 4 and 5 are capable of carrying out this henry reaction. And Entry 6 in this table, starting with solvent, acid catalyst part and final product: β-nitrostyrene, suggests acid-catalyst cannot drive the reaction backward either. As a result, those data indicate that we need both phosphonic acid and cinchonidine to promote this Deacetalization-Henry cascade reaction.

By the addition of both acid and base functional groups as catalysts, Deacetalization-Henry cascade reactions were performed. As shown in **Table 3.9**, bifunctional heterogeneous catalyst designed exhibited successfully promoted this cascade reaction, giving a

100% conversion of reactant and a yield of 54% for β-nitrostyrene. Besides, if we applied a longer Uv/O_3 exposure in **Table 3.9**, entry 2, due to the lack of efficient phosphonic acid groups to carry out deacetalization step, both the conversion and yield of final product observed appear a dramatic decrease.

In Entry 3 to Entry 6 of **Table 3.9**, Physical mixture A represents a mixture of **Cd-SBA15** and **H_2O_3P-SBA15** with same amount of acid and base group with 50mg **Cd-Uv-H_2O_3P-SBA15-3h** while Physical mixture B is the same with 50mg **Cd-Uv-H_2O_3P-SBA15-5h**. However, compared with bifunctional catalysts, physical mixtures exhibited a better performance in deacetalization-Henry cascade reaction.

The reason for the difference between bifunctional catalyst and physical mixture of two mono-functional catalysts (or the loss of activity) might be the loss of surface silanol groups. Brunelli et al. have reported a similar decreased activity in aldol condensation when they cooperated amine groups with carboxylic acid on silica.[33] They proposed that silanol will better cooperatively catalyzing the aldol condensation than acid. To investigate our case, some more reactions were performed in **Table 3.10** , as we silylated silanol groups on SBA-15 surface with hexamethyldisilazane (HMDS). First, Entry 6 indicates that HMDS capped plain **SBA-15** has no increased catalytic activity on nitromethane addition. Then the remaining silanol groups on **Cd-SBA15** were silylated with HMDS (**HMDS-Cd-SBA15**). As shown in Entry 1 to Entry 5 in **Table 3.10**, **Cd-SBA15** with silylation shows a similar catalytic performance with bifunctional catalyst (**Cd-Uv-H_2O_3P-SBA15-3h**) and the same lower activity when compared with **unsilylated Cd-SBA15**. It suggests that loss of silanol will also cause a significant loss of activity for cinchonidine

functionalized catalyst in this henry reaction. That would be the key reason that our bi-functional catalyst has lower performance than physical mixture.

The turnover frequency for each step was then calculated in **Table 3.11** with the phosphonic and cinchonidine contents from **Table 3.5.** A lower TOF for basic moiety can be observed in this case. The steric hindrance caused by this relatively larger cinchonidine group may be one of the reasons. More studies need to be conducted to optimize this tandem reaction rate since basic sites, the concentration of the intermediate (benzaldehyde)[34] produced by acidic sites, and surface silanols are all related to the final reaction rate.

Last, the recyclability of our acid-base bifunctional catalyst **Cd-Uv-H_2O_3P-SBA15-3h** was tested. After each run, the catalyst was filtered and washed with toluene, dried in vacuum overnight, and reused. The results shown in **Figure 3.9** illustrates the **Cd-Uv-H_2O_3P-SBA15-3h** remains about 80% efficiency after five consecutive catalytic uses for Deacetalization-Henry reaction.

Table 3.7. Catalytic activity testing for Deacetalization reaction(acid-catalyzed step).
Catalytic reaction: **catalyst(different weight)**, nitromethane 4 ml and benzaldehyde dimethyl acetal 0.5 mmol. React at 90 °C under nitrogen atmosphere for different time. *Yield of **3**= conversion of **1** * selectivity of **3***
[a] As for a blank test, no catalyst was added to system.
[b] Same base content with Cd-Uv-H_2O_3P-SBA15-3h
[c] Same acid content with Cd-Uv-H_2O_3P-SBA15-3h
[d] Use for TOF calculation

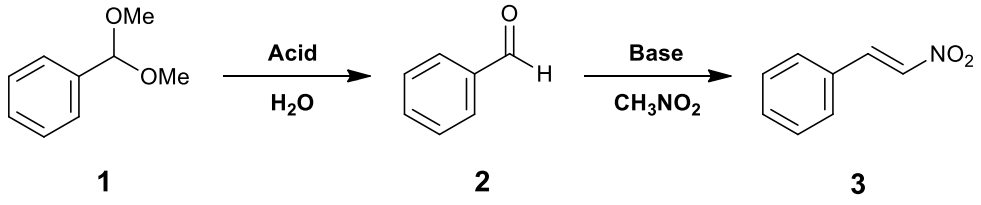

Entry	Sample	Time /h	Conversion of **1** /%	Yield of **3**/%
1	Blank test [a]	12	5	0
2	13.6mg pristine-SBA15	12	7	0
3	16.3 mg Cd-SBA15 [b]	12	0	0
4	13.6mg H_2O_3P-SBA15 [c]	1.5	100	0
5	5mg H_2O_3P -SBA15 [d]	0.5	46	0

Table 3.8 Catalytic activity testing for Henry Reaction between Benzaldehyde and Nitromethane(base-catalyzed step). Catalytic reaction: **catalyst(different weight)**, nitromethane 4 ml and benzaldehyde 0.5 mmol. React at 90 °C under nitrogen atmosphere for different time
[a] As for a blank test, no catalyst was added to system.
[b] Same acid content with Cd-Uv-H_2O_3P-SBA15-3h.
[c] Same base content with Cd-Uv-H_2O_3P-SBA15-3h. Use for TOF calculation.
[d] Starting from nitromethane 4 ml and 0.5mmol final product(β-nitrostyrene, **3** in scheme 3), which means the initial conversion and selectivity are 100%. Then 13.6mg H_2O_3P-SBA15 was added as catalyst. And after 6h, there is no conversion from nitroalkene back to benzaldehyde, suggests acid-catalyst cannot drive the reaction backward.

Entry	Sample	Time /h	Conversion of **2** /%	Yield of **3**/%
1	Blank test [a]	6	0	0
2	16.5mg SBA15	6	0	0
3	H_2O_3P-SBA15 [b]	12	0	0
4	Cd-SBA15 [c]	3	17	~100
5	Cd-Uv-H_2O_3P-SBA15-3h	24	85	~100
6	H_2O_3P-SBA15 [d]	6	100	100

Table 3.9. Catalytic activity testing for Deacetalization-Henry cascade reaction. Monitored by GC. Catalytic reaction: Catalyst, nitromethane 4 ml and benzaldehyde dimethyl acetal 0.5 mmol. React at 90 ℃ under nitrogen atmosphere for different times. The results in 24h are shown in the figure(below the table) for comparison.
Catalysts: 50 mg Cd-Uv-H_2O_3P-SBA15-3h for entry 1. Physical mixture A: a mixture of **16.3mg** Cd-SBA15 and **13.6mg** H_2PO_3-SBA15. Physical mixture B: a mixture of **35.0mg** Cd-SBA15 and **5.0mg** H2PO3-SBA15.

Entry	Sample	Time /h	Conversion of **1**/%	Selectivity of **2**/%	Selectivity of **3**/%	Absolute conversion of **3** /%
1	Cd-Uv-H_2O_3P-SBA15-3h	24	100	46	54	54
2	Cd-Uv-H_2O_3P-SBA15-5h	24	36	44	56	20
3	Physical mixture A	3	44	66	34	15
4	Physical mixture A	24	100	2	98	98
5	Physical mixture B	3	14	50	50	7
6	Physical mixture B	24	34	9	91	32

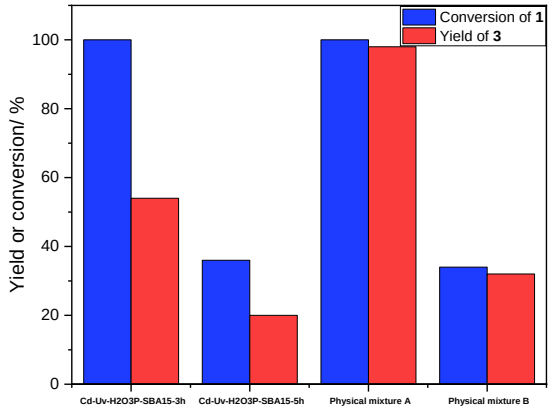

Catalytic activity testing in 24h

Table 3.10 Catalytic activity testing for Henry reaction. Monitored by GC. Catalytic reaction: Catalysts with same amount of cinchonidine content with 50mg Cd-Uv-H_2O_3P-SBA15-3h, nitromethane 4 ml and benzaldehyde 0.5 mmol. React at 90 ℃ under nitrogen atmosphere for different times. The results in both 6h and 24h are shown in the figure below for comparison.

Entry	Sample	Time/h	Yield of **3**/%
1	Cd-Uv-H_2O_3P-SBA15-3h	6	15
2	HMDS-Cd-SBA15	6	20
3	Cd-Uv-H_2O_3P-SBA15-3h	24	42
4	HMDS-Cd-SBA15	24	47
5	Cd-SBA15	6	39
6	HMDS-SBA15	6	0

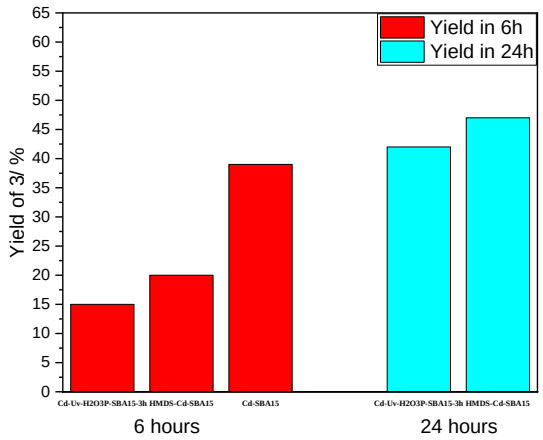

Table 3.11 Kinetic constant(TOF) calculation. Catalytic reaction: catalyst, nitromethane 4 ml and different starting reactant. React at 90 ℃ under nitrogen atmosphere for different times.
[a] 5mg H_2O_3P-SBA15 was added as catalyst, starting from **benzaldehyde dimethyl acetal** 0.5 mmol
[b] 16.5mg Cd-SBA15 was added as catalyst, starting from **benzaldehyde** 0.5 mmol.
[c] TOF=moles of reactant*conversion/(moles of active sites*time). Mole of reactant is 0.5mmol to both entry 1 and 2

Entry	Sample	Time/h	Conversion/%	TOF /s^{-1} [c]
1	H_2O_3P-SBA15 [a]	0.5	46	$4.20*10^{-2}$
2	Cd-SBA15 [b]	3	17	$6.86*10^{-4}$

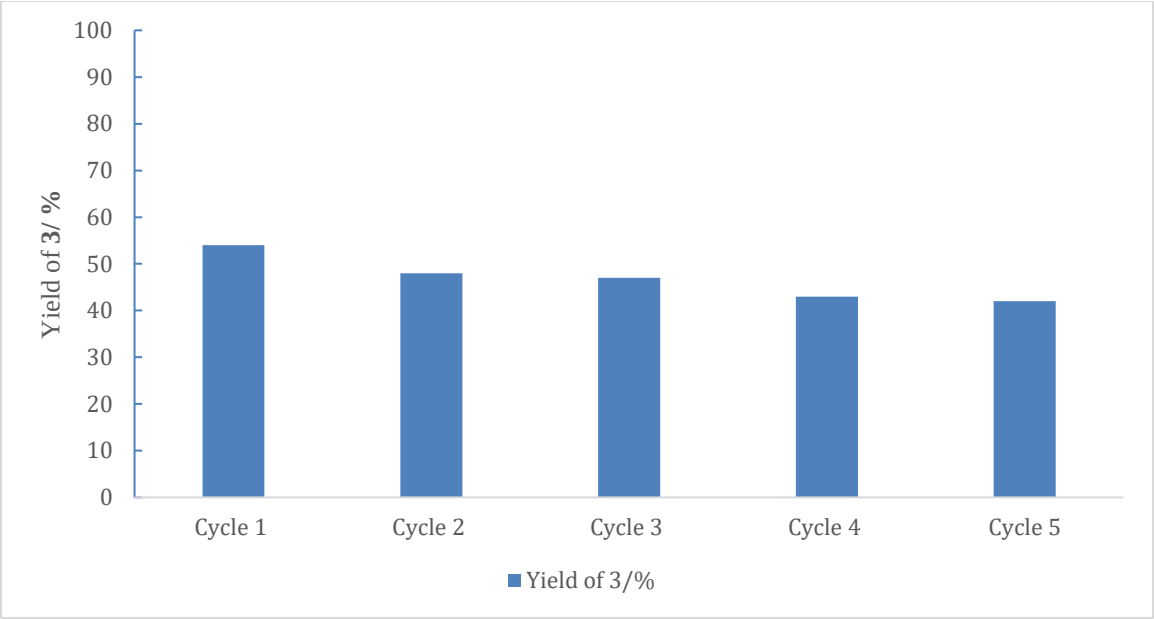

Figure 3.9 Recyclability test for Deacetalization-Henry cascade reaction.

3.6.2 Cyano-Ethoxycarbonylation reaction

One reason for developing our 2nd-generation acid-base catalyst is to add more functionalities and enlarge the range capable reaction for catalysts so the performance of our 2nd-generation acid-base catalyst of Cyano-Ethoxycarbonylation reaction was examined. The results are summarized in **Table 3.12**.

One reason for choosing Cyano-Ethoxycarbonylation reaction is this reaction can be promoted by high nucleophilicity Lewis base catalyst (e.g. DABCO, DMAP….).[35-37] An acid-base cooperative function has also been recently reported to have an enhanced performance on it.[38,39] But the primary amine (NH_2-) in our 1st-generation catalyst has no effect on this reaction, as shown in Entry 3 in **Table 3.12** since a tertiary amine (NR_3) is favored for carrying out this catalysis.

Entry 1 to Entry 3 in **Table 3.12** indicate that blank test, **SBA-15** (silica support) and our 1st-generation acid-base catalyst have no effect on promoting this Cyano-Ethoxycarbonylation reaction at all. In contrast, the 2nd-generation acid-base catalyst, **Cd-Uv-H_2O_3P-SBA15-3h** in Entry 4 exhibits a 40% yield of cyano carbonate in 30h. Further, different from Deacetalization-Henry cascade reaction, **Cd-Uv-H_2O_3P-SBA15-5h** represents a better performance on this reaction, with a yield of 61%. Both the inherent difference between cascade reaction and dual activate reaction, and more post-grafted cinchonidine content due to longer Uv/ozonolysis treatment, which plays a key role in cyano-ethoxycarbonylation, may attribute to this higher product yield.

Entry 6 and 7 are the physical mixture of **Cd-SBA15** and **H_2O_3P-SBA15** with same cinchonidine and phosphonic acid amount with **Cd-Uv-H_2O_3P-SBA15-3h** and **Cd-Uv-**

H_2O_3P-SBA15-5h, respectively. Different with a much higher yield than their bifunctionalized material in Deacetalization-Henry discussed in the last part, physical mixtures only show a quite similar yield of cyano carbonate in this case. As we discussed above, surface silanols on support may also have a promotive effect together with functional (basic) sites in some reactions. And this similar results shown in this table indicate surface silanols of SBA-15, pure silica, have few effects on promoting Cyano-Ethoxycarbonylation reaction. This may mostly result from the acidity of pure silica silanols is insufficient to serve as a good reactant activator. However, by increasing Lewis acidity of surface silanols, for example, cooperating metal oxide (Al_2O_3….) into framework, base-functionalized "acidic" silica did exhibit a good activity in Cyano-Ethoxycarbonylation reaction for a synergistic acid silanol-base catalysis.[40]

The recyclability test of **Cd-Uv-H_2O_3P-SBA15-5h**, which represents a higher catalytic activity, was also performed. After each run, the catalyst was filtered and washed with toluene, dried in vacuum overnight, and reused. Results are shown in **Figure 3.10**. Despite a slight loss of activity, **Cd-Uv-H_2O_3P-SBA15-5h** also remains ~80% performance after five consecutive runs (Activity drop from 61% to about 50%). Those data confirm our bifunctional catalysts are recyclable.

As the scheme in **Table 3.12**, this reaction will create a chiral center at the cyano added carbon. Unfortunately, all entries we mentioned above only generate racemic products. Those racemic products probably indicate that in our cinchonidine-phosphonic acid cooperative function, enantioselective addition comes from acidic sites. A similar situation and a proposed mechanism have been reported by Yamagiwa et al.[41] On the other hand, it

also proves that in our construction, acidic and basic site are well spatially isolated. Those grafted functionalities maintained their original characters well but the chirality of cinchonidine (basic sites) won't be introduced to phosphonic acid located at the inner position, which might also be a drawback of our spatially isolated methodology in dual-activation chiral reaction application.

For entry 8 in **Table 3.12**, we only applied Cinchonidine mono-functionalized catalyst for this reaction. Lacking acid sites working cooperatively, **Cd-SBA-15** only appears a low yield of 22% in 30h with same amount of basic sites participating as other entries. However, it provides a ~15% enantiomeric excess value due to the reaction only activate or catalyzed on chiral cinchonidine groups.

Table 3.12 Cyano-Ethoxycarbonylation reaction catalyzed by acid-base bifunctional catalyst.
Reaction condition: toluene 2.5ml, ethyl cyanoformate (0.5mmol), and benzaldehyde (0.25 mmol), 8 mol% amount(based on benzaldehyde) of catalyst was added (0.020mmol cinchonidine). The mixture was vigorously stirred at room temperature under N2 for 30h and analyzed by GC-MS. ee% values are obtained from GC with chiral column.
[a] No catalyst was added for a blank test
[b] 8 mol% amount(based on benzaldehyde) of catalyst was added: 90mg Cd-Uv(H_2PO_3-SBA15)-3h or 46.7 Cd-Uv(H_2PO_3-SBA15)-5h.
[c] Yield of product was based on benzaldehyde.
[d] Physical mixture has an **equal** amount of cinchonidine and phosphorous acid with 90mg Cd-Uv(H_2PO_3-SBA15)-3h(29.3mg Cd-SBA15 and 24.5mg H_2PO_3-SBA15)
[e] Cd-SBA15 has a 15% ee. ee% values are obtained from GC with chiral column.

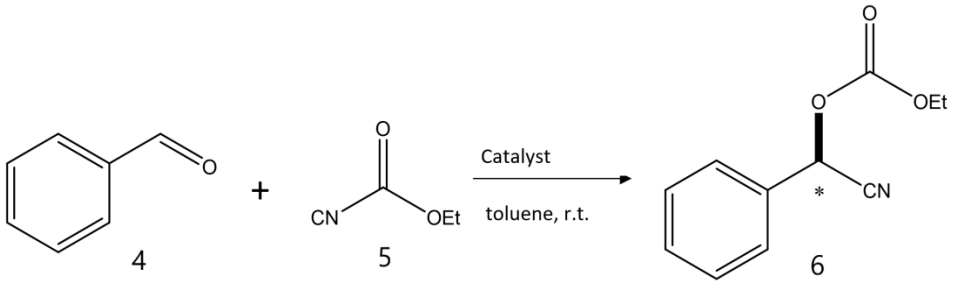

Entry	Sample	Time/h	yield of **6** [c] /%
1	Blank Test [a]	30	~0
2	Pristine-SBA15	30	~0
3	HSO_3-(NH_2-SBA-15)	30	~0
4	Cd-Uv(H_2PO_3-SBA15)-3h [b]	30	40
5	Cd-Uv(H_2PO_3-SBA15)-5h [b]	30	61
6	Physical mixture for 3h [d]	30	35
7	Physical mixture for 5h [d]	30	72
8	Cd-SBA15	30	22[e]

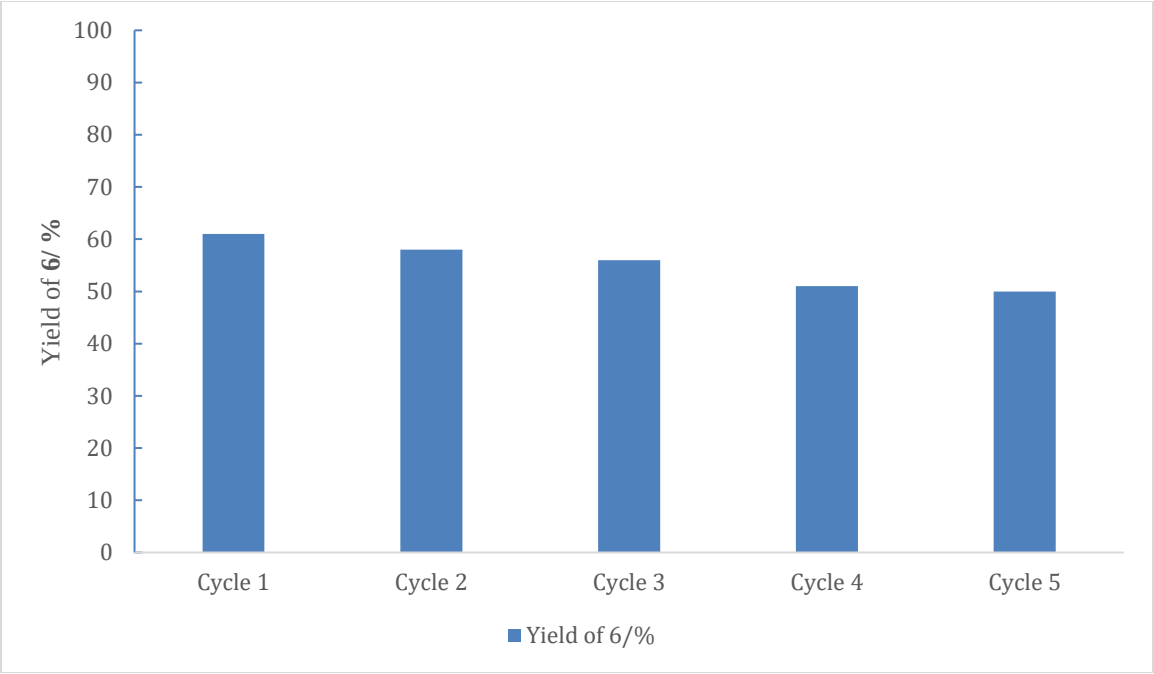

Figure 3.10 Recyclability test for Cyano-Ethoxycarbonylation reaction.

3.6.3 1,4-addition of thiols to cylic enones

1,4-addition of thiols to cylic enones, which is sometimes called Sulfa-Michael addition, has a significant impact on the development of asymmetric catalysis by cinchona alkaloids.[42] It can be promoting with help of bases and similar with some other Michael addition, the performance of it can be further improved with the participation of acid. Our 2nd-Generation Dual Acid−Base Catalysts acid−base catalysts were tested with this reaction and the results of all materials are shown in **Table 3.13**. All reactions were performed with 1% mol catalyst at room temperature for 24 hours.

Blank test and Pristine **SBA-15** shows a poor effect on sulfa-Michael addition and at the same time, acid catalyst alone (**H_2O_3P-SBA15** in entry 7) also only shows a very low yield for 10% and produced some by-product. It may indicate the necessity of basic moieties addition for carrying out promotion this reaction.

By adding cinchonidine functionalities as a catalyst into reaction system, the reaction can be successfully promoted as entry 3 to entry 6 shown. In entry 3, cinchonidine solid was directly introduced into benzene solution, providing almost 100% conversion and the highest ee% for 40% in 24h. Chiral-base modified SBA15, **Cd-SBA-15** and the physical mixture of **Cd-Uv(H_2PO_3-SBA15)-3h** both show a good conversion for 69% and 83%, respectively. And the better yield of physical mixture indicates that the cooperative work of acid and base function did improve catalytic activity. However, there is a loss of enantioselectivity in both materials compared with free cinchonidine in solution. It may relate with the removal of the OH group in the cinchonidine upon derivatization since it has

been reported that this C9-OH group allows a simultaneous activation which attributes to a high enantioselectivity.[42,43]

Performances of bifunctional catalyst, **Cd-Uv(H_2PO_3-SBA15)-3h**, were shown in entry 7. The conversion was similar to Cd-SBA15. Like Deacetalization-Henry cascade reaction we discussed above, silanols might have some effect on its rate.[19] The improved activity by introducing acid sites was somewhat canceled by the loss of silanols, which may be the main reason for this similar yield. However, until now, the mechanism of cinchonidine catalyzed sulfa-Michael addition has not been fully discovered yet.

Besides, It can be observed that a slightly lower ee% of **Cd-Uv(H_2PO_3-SBA15)-3h** and physical mixture appear when compared with Cd-SBA15. That may most probably due to the non-chiral phosphonic acid groups, which cooperatively promoted the reaction but without any enantioselectivity. Besides, phosphonic can catalyzed this reaction itself as **Table 3.13** shown. That may further dilute the overall e.e. observed.

Table 3.13 1,4-addition of thiols to cylic enones reaction catalyzed by acid-base bifunctional catalyst. Reaction condition: benzene 3ml, p-tertbutylbenzenethiol (1.81mmol), and 2-cyclohexene-1-one (1.56 mmol), 1 mol% amount(based on ketone) of catalyst was added (0.015mmol cinchonidine). The mixture was vigorously stirred at room temperature under N_2 for 24h and analyzed by GC. ee% values are obtained from MC 241 polarimeter.

[a] No catalyst was added for a blank test

[b] 1 mol% cinchonidine was directly added into solution as catalyst.

[c] Yield of product was based on ketone.

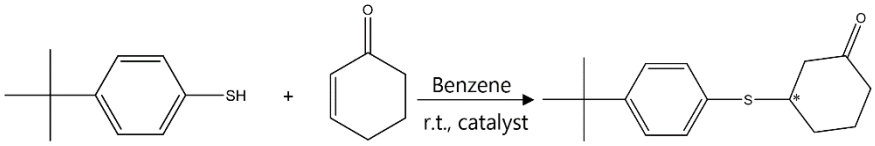

Entry	Sample	Time/h	yield of **product** [c] /%	ee%
1	Blank Test [a]	24	~0	N/A
2	Pristine-SBA15	24	6	trace
3	Cinchonidine[b]	24	~100	40
4	Cd-SBA15	24	69	10
5	Physical mixture for 3h	24	83	4
6	Cd-Uv(H_2PO_3-SBA15)-3h	24	70	6
7	H_2O_3P-SBA15	24	10	trace

3.6.4 Reaction Limitations

By utilizing our phosphorous-Cinchonidine bifunctional catalyst, we have successfully promoted Deacetalization-Henry cascade reaction, Cyano-Ethoxycarbonylation reaction and 1,4-addition of thiols to cylic enones. However, since grafted functional groups are simply phosphorous acid and cinchonidine, natural cinchona alkaloids, both are very "primary" and "undecorated", its applications were limited. Our bifunctional catalysts prepared show very little activity on Michael addition reactions of unmodified aldehydes or ketones.[44] This base-catalyzed nucleophilic addition to an α,β-unsaturated carbonyl compound is widely used in asymmetric synthesis (for example, **Figure3.11**). Besides, like the reaction scheme shown in **Figure3.12**, the chiral base-catalyzed Morita-Baylis-Hillman coupling is also related to Michael addition since MBH coupling involves a sequence of Michael addition, aldol reaction, and β-elimination.[45] Unfortunately, cinchonidine is not a good catalyst for this kind of Michael addition. A secondary amine, not quaternary amines in cinchonidine, will be preferred in this case by enabling an enamine or iminium activation step.[46-48] As a result, neither our catalysts nor a cinchonidine grafted SBA15 showed any effect on the reactions shown in **Figure3.11** and **3.12**. In future studies, some modification might be required for those natural cinchona alkaloids moieties to further enhance their catalytic performance on those reactions.

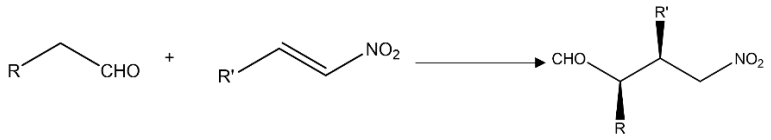

Figure3.11 Scheme for Michael addition of unmodified aldehydes to nitro olefins.

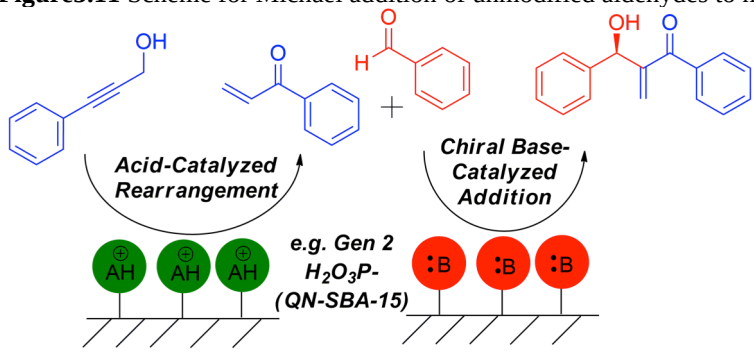

Figure3.12 Scheme for Meyer-Schuster rearrangement followed by a subsequent chiral Morita-Baylis-Hillman coupling

3.7 Conclusion

A 2nd-generation dual acid−base system was constructed by combining our UV/ozonolysis removal protocol and "click" chemistry, with phosphonic acid and cinchonidine serves as acidic and basic sites, respectively. Our new approaches are based on: (1) the use of “click” chemistry to immobilize molecular moieties to oxide surfaces via intermediate alkyltrialkoxysilane (R-TEOS) linkers; (2)controlled use of UV/ozonolysis for partial removal of tethered fragments from the external surface; (3) the use of ethoxy protecting groups to avoid quenching between incompatible acidic and basic functionalities. ^{13}C, ^{29}Si and ^{31}P solid-state NMR were combined with CNS elemental analysis, acid−base titrations and N_2 adsorption isotherm measurements to fully characterize those resulting materials. The successful construction work for 2nd-generation acid-base catalyst further confirmed that this synthetic protocol is fairly general and could be applied for designing other bifunctional catalysts. Besides, the recovery process of silanols via UV/O_3 treatment was investigated.

The dual functionalities were tested with Deacetalization-Henry cascade reaction, Cyano-Ethoxycarbonylation reaction and 1,4-addition of thiols to cylic enones (Sulfa-Michael addition). A decrease in catalytic activity for bifunctional catalysts, compared with physical mixture, have been observed in Deacetalization-Henry cascade reaction, due to the loss of cooperatively catalyzing surface silanol groups for henry reaction. In the meanwhile, similar performance for bifunctional catalysts and their physical mixture can be observed for the insufficient acidity of pure silica surface silanols. Bifunctional catalysts could be recycled for those reactions, with a ~80% total activity remaining after five

cycles. In 1,4-addition of thiols to cylic enones, a slightly increased activity could be found in physical mixture caused by extra silanol, again, for its weak acidity. There is a loss of enantioselectivity in both Cyano-Ethoxycarbonylation reaction and 1,4-addition of thiols to cylic enones, which may be caused by weak cooperative working due to spatially isolated structure and non-chirality acidic moieties grafted, respectively.

References

1. A. Feinle, S. Flaig, M. Puchberger, U. Schubert, N. Husing, "Stable Carboxylic Acid Derivatized Alkoxy Silanes", Chem. Commun. 51 (2015) 2339-2341.

2. Kaufman TS, Ru´veda EA (2005) Angew Chem Int Ed 44:854

3. Ashley E, McGready R, Proux S, Nosten F (2006) Travel Med Infect Dis 4:159

4. White NJ (2007) Lancet Infect Dis 7:549

5. Meyer CG, Marks F, Hay J (2004) Trop Med Int Health 9:1239

6. La¨mmerhofer M, Lindner W (2008) Adv Chromatog 46:1

7. Kacprzak, K.; Gawronski, J., Resolution of Racemates and Enantioselective Analytics by Cinchona Alkaloids and Their Derivatives. In Cinchona Alkaloids in Synthesis and Catalysis: Ligands, Immobilization and Organocatalysis; Song, C. E., Ed.; Wiley-VCH: Weinheim, Germany, 2009.

8. Wynberg H (1986) Top Stereochem 16:87

9. Kim, S. G.; Han Ahn, K. Tetrahedron Lett. 2001, 42 (25), 4175–4177

10. Kacprzak K Gawron´ski J (2001) Synthesis 961

11. Mallat T, Orglmeister E, Baiker A (2007) Chem Rev 107:4863

12. Ma Z, Zaera F (2009) Chiral modification of catalytic surfaces. In: Ozkan US (ed) Design of heterogeneous catalysis: new approaches based on synthesis, characterization, and modelling. Wiley-VCH, Weinheim, pp 113–140

13. Notestein JM, Katz A (2006) Chem Eur J 12:3954

14. Cope´ret C, Basset J-M (2007) Adv Synth Catal 349:78

15. Corma A, Garcia H (2006) Adv Synth Catal 348:1391

16. Margelefsky EL, Zeidan RK, Davis ME (2008) Chem Soc Rev 37:1118

17. Lindholm A, Maki-Arvela P, Toukoniitty E, Pakkanen TA, Hirvi JT, Salmi T, Murzin DY, Sjoholm R, Leino R (2002) J Chem Soc Perkin Trans 1:2605

18. Hong, J.; Lee, I.; Zaera, F. Top. Catal. 2011, 54 (19–20), 1340–1347.

19. Hong, J.; Zaera, F. J. Am. Chem. Soc. 2012, 134 (31), 13056–13065.

20. Ellebracht, N. C.; Jones, C. W. ACS Catal. 2019, 9 (4), 3266–3277.

21. Wang Y.-L., Zhu L., Guo B.-L., Chen S.-W., Wu W.-S., New J. Chem. 38 (2014) 3853-3861.

22. Pan, Y. C.; Gavin Tsai, H. H.; Jiang, J. C.; Kao, C. C.; Sung, T. L.; Chiu, P. J.; Saikia, D.; Chang, J. H.; Kao, H. M. J. Phys. Chem. C 2012, 116 (2), 1658–1669.

23. Vig, J. R. UV/Ozone Cleaning of Surfaces. J. Vac. Sci. Technol., A 1985, 3, 1027−1034.

24. Guo, L.; Zaera, F. Spatial Resolution in Thin Film Deposition on Silicon Surfaces by Combining Silylation and UV/Ozonolysis. Nanotechnology 2014, 25, 504006.

25. Moreland, C. G.; Philip, A.; Carroll, F. I. J. Org. Chem. 1974, 39 (16), 2413–2416.

26. Kõllo, M.; Kudrjašova, M.; Kulp, M.; Aav, R. Anal. Methods 2013, 5 (16), 4005–4009.

27. Palomo, C.; Oiarbide, M.; Laso, A. Recent Advances in the Catalytic Asymmetric Nitroaldol (Henry) Reaction. Eur. J. Org. Chem.2007, 2007, 2561−2574.

28. Guan, J.; Liu, B.; Yang, X.; Hu, J.; Wang, C.; Kan, Q. Immobilization of Proline onto Al-SBA-15 for C−C Bond-Forming Reactions. ACS Sustainable Chem. Eng. 2014, 2, 925−933.

29. Ide, M.; El-Roz, M.; De Canck, E.; Vicente, A.; Planckaert, T.; Bogaerts, T.; Van Driessche, I.; Lynen, F.; Van Speybroeck, V.; Thybault-Starzyk, F.; Van Der Voort, P. Phys. Chem. Chem. Phys. 2013, 15 (2), 642–650.

30. Huang, Y.; Xu, S.; Lin, V. S. Y. Bifunctionalized Mesoporous Materials with Site-Separated Brønsted Acids and Bases: Catalyst for a Two-Step Reaction Sequence. Angew. Chem., Int. Ed. 2011, 50, 661−664.

31. Guan, J.; Liu, B.; Yang, X.; Hu, J.; Wang, C.; Kan, Q. Immobilization of Proline onto Al-SBA-15 for C−C Bond-Forming Reactions. ACS Sustainable Chem. Eng. 2014, 2, 925−933.

32. Biradar, A. V.; Patil, V. S.; Chandra, P.; Doke, D. S.; Asefa, T. A Trifunctional Mesoporous Silica-Based, Highly Active Catalyst for One-Pot, Three-Step Cascade Reactions. Chem. Commun. 2015, 51,8496−8499.

33. Brunelli, N. A.; Venkatasubbaiah, K.; Jones, C. W. Chem. Mater. 2012, 24 (13), 2433–2442.

34. Weng, Z.; Yu, T.; Zaera, F. ACS Catal. 2018, 8 (4), 2870–2879.

35. Deardorff, D.R.; Taniguchi, C.M.; Tafti, S.A.; Kim, H.Y.; Choi, S.Y.; Downey, K.J.; Nguyen, T.V. J. Org. Chem. 2001, 66, 7191–7194.

36. Hoffmann, H.M.R.; Ismail, Z.M.; Hollweg, R.; Zein, A.R. Bull. Chem. Soc. Jpn. 1990, 63, 1807–1810.

37. Aoki, S.; Kotani, S.; Sugiura, M.; Nakajima, M. Tetrahedron Lett. 2010, 51, 3547–3549.

38. Chinchilla, R.; Nájera, C.; Ortega, F. J. Tetrahedron Asymmetry 2008, 19 (3), 265–268.

39. Matsukawa, S.; Kimura, J.; Yoshioka, M. Molecules 2016, 21 (8).

40. Motokura, K. J. Japan Pet. Inst. 2014, 57 (3), 95–108.

41. Yamagiwa, N.; Tian, J.; Matsunaga, S.; Shibasaki, M. J. Am. Chem. Soc. 2005, 127 (10), 3413–3422.

42. Hiemstra, H.; Wynberg, H. J. Am. Chem. Soc. 1981, 103 (2), 417–430.

43. Tian, S. K.; Chen, Y.; Hang, J.; Tang, L.; McDaid, P.; Deng, L. Acc. Chem. Res. 2004, 37 (8), 621–631.

44. Michael A., Für Prakt J. Chem. 1887, 35, 349.

45. Jin, R.; Zheng, D.; Liu, R.; Liu, G. ChemCatChem 2018, 10 (8), 1739–1752.

46. Betancort, J. M.; Barbas, C. F. Org. Lett. 2001, 3 (23), 3737–3740.

47. Mase, N.; Thayumanavan, R.; Tanaka, F.; Barbas, C. F. Org. Lett. 2004, 6 (15), 2527–2530.

48. Yang, S.; He, J. Chem. Commun. 2012, 48 (83), 10349–10351.

Chapter 4: A Summary for Constructing Acid-Base Heterogeneous Tandem Catalysts

Overall, the construction of two generations of acid-base heterogeneous tandem catalysts are successfully performed as Chapter 2 and 3 shown. A series of characterization technique including: ^{13}C, ^{29}Si and ^{31}P solid-state NMR, infrared spectroscopy(IR), acid-base titration, CNS elemental analysis, and N_2 adsorption-desorption isotherm measurement were employed. Those analytic results corroborate not only the existence of functionalities on SBA-15 support but also the success of each individual step associated with this synthesis.

Besides, two different semi-quantitative measurements were discussed in the ^{29}Si NMR part of Chapter 2 and N_2 adsorption-desorption isotherm part in Chapter 3, respectively. For the ^{29}Si NMR spectra of sulfonic acid-amine tandem catalyst, we observed the trend of absolute functionalities content obtained from titrations well matched that of T peak area percentage, which represents how many Si on support were tethered. For N_2 adsorption-desorption isotherm part, bimodal shapes in pore size distribution were found in both systems and more clearly in cinchonidine-phosphonic acid tandem catalyst due to a larger difference in moiety size. After multi-peak Gaussian fitting for pore size distribution, it was observed that the relative change for pore at 5.41nm agreed with the changing trend of absolute acid content. Anyway, without systemic studies, those semi-quantitative analysis should be taken with a grain of salt.

In the study of 1st-generation acid−base tandem catalyst derivatized with amine(-NH_2) and sulfonic acid(-HSO_3), we found that the overall ratio of the coverages of the two functionalities on the surface can be controlled by tuning UV/ ozonolysis exposure length, which more detailed works are produced by Dr. Zhihuan. It can be applied to optimize the performance for Deacetalization-Henry cascade reaction. Thanks to spatially separated moieties and proper acid/base ratio, catalysts with 3-hour Uv/Ozonolysis exposure (**HSO_3-(NH_2-SBA-15)**) displays the best performance among all catalysts prepared, where a 98% yield of β-nitrostyrene was achieved in 13 hours.

In the study of catalytic performance for 2nd-generation cinchonidine-phosphonic acid system, a decrease in catalytic activity for bifunctional catalysts, compared with physical mixture, have been observed in Deacetalization-Henry cascade reaction, which has not been observed in 1st-generation acid−base tandem catalyst. The difference should come from the different catalytic systems for two bifunctional catalysts. And similar to previously reported, such a decreased activity was most probably due to the loss of cooperatively catalyzing surface silanol groups for henry reaction after our complementary tests. Thanks to extra functionalities introduced by cinchonidine moieties, 2nd-generation bifunctional catalysts successfully promoted Cyano-Ethoxycarbonylation reaction and Sulfa-Michael reaction which 1st-generation couldn't. However, there is a loss of enantioselectivity in both Cyano-Ethoxycarbonylation reaction and 1,4-addition of thiols to cylic enones. Weaker cooperative working due to spatially isolated structure and the non-chirality of acidic moieties may both attribute to it.

Last, Recyclability was examined from both tandem catalysts prepared and they remained good catalytic activity after a couple of consecutive runs (For **HSO_3-NH_2-SBA-15**, a drop of ~5% in total activity, was seen after three cycles by Dr.Zhihuan's work and for **Cd-Uv(H_2PO_3-SBA15)-3h,** ~80% of catalytic activity still remained after five cycles.)

A more important idea we want to deliver from this thesis is the synthetic strategy protocol. Both partial removal process from Uv/O_3 treatment and tethering route via a R-TEOS link could be applied for constructing a similar tandem system without many limitations.

Anyway, there are still issues that need to be resolved for this acid-base tandem catalyst in the future. One issue is for Uv/O_3 ozonolysis removal process. In our study, we found this removal process cannot clean functional moieties with phenyl groups. Probably due to the deep tunnel shape for SBA-15 comparing with a silicon film, which is difficult for ozone to access and high carbon content for phenyl groups, those moieties will "coke" on silica support instead of being removed. That is also one reason why in our 2nd-generation catalyst, DEP- functionality is grafted first, then Cd- group tethered. Another thing is both acidic and basic moieties we grafted need to be re-considered. For example, cinchonidine is a good chiral basic moiety but it was blocked for Michael addition after our test. The tertiary amines it owns do not allow cinchonidine to follow an enamine activation route. Such a low catalytic activity on Michael addition limited its application on asymmetric reactions. So for future studies, decorated cinchona alkaloids or other secondary amine contained basic functionalities may be a better choice. The same thing for acid moieties, carboxylic acid which can be grafted by carboxylic-acid tert-butyl ester-linked triethoxysilanes seems to be a better choice compared with the other two acid mentioned in thesis.

N_2 flow heating deprotection process of this carboxylic acid moiety will make it compatible for more types of bases even if those bases are not protected. More experiments need to be conducted next and we hope to solve these issues in near future.